UC San Diego

UC San Diego Electronic Theses and Dissertations

Title

Uptake Kinetics of a Pure α-Pinene-Derived Hydroxy Nitrate onto Seed Aerosol at Different Relative Humidity and Particle Acidity

Permalink

https://escholarship.org/uc/item/4d59d8z8

Author

Kawasaki, Allison Mayumi

Publication Date

2022

Peer reviewed|Thesis/dissertation

UNIVERSITY OF CALIFORNIA SAN DIEGO

Uptake Kinetics of a Pure α-Pinene-Derived Hydroxy Nitrate onto Seed Aerosol at Different

Relative Humidity and Particle Acidity

A Thesis submitted in partial satisfaction of the requirements
for the degree Master of Science

in

Chemistry

by

Allison Mayumi Kawasaki

Committee in charge:

    Professor Jonathan Slade, Chair
    Professor Robert Pomeroy
    Professor Erik Romero

2022

The Thesis of Allison Mayumi Kawasaki is approved, and it is acceptable in quality and form for publication on microfilm and electronically.

University of California San Diego

2022

DEDICATION

For my Mom and Dad. I love you forever.

TABLE OF CONTENTS

LIST OF FIGURES

LIST OF TABLES

ACKNOWLEDGEMENTS

I want to thank all my family and friends for their endless love and support. My roommates Daisy and Tara and my best friend Lucy for always being there to help me through graduate school. All my lab mates for their assistance and ideas with research. I would like to thank my thesis advisor Dr. Slade for all his advice and guidance. Finally, I'd like to thank my good friend Ritchie for all his assistance with my research.

VITA

2019   Bachelor of Science in Environmental Chemistry, University of California San Diego

2022   Master of Science in Chemistry, University of California San Diego

ABSTRACT OF THE THESIS

Uptake Kinetics of a Pure α-Pinene-Derived Hydroxy Nitrate onto Seed Aerosol at Different

Relative Humidity and Particle Acidity

by

Allison Mayumi Kawasaki

Master of Science in Chemistry

University of California San Diego, 2022

Professor Jonathan Slade, Chair

Organic nitrates, produced from the oxidation of biogenic volatile organic compounds

(BVOC) in the presence of nitrogen oxides (NO_x), have significant contributions to the global

secondary organic aerosol (SOA) budget and slow the production of ozone by sequestering NO_x.

Monoterpenes, such as α-pinene, are important organic nitrate and SOA precursors and are the

second largest contributor to non-methane BVOC mass next to isoprene. It has been observed in

previous studies that α-pinene-derived hydroxy nitrates readily partition to the particle phase,

introducing a potential sink for atmospheric NO_x through reactions such as acid-catalyzed

hydrolysis. However, the role of relative humidity and particle acidity in the mass accommodation and rate of uptake of hydroxy nitrates by aerosol are not well understood, introducing a knowledge gap in the fate of atmospheric NO_x. In this experiment, an α-pinene hydroxy nitrate is synthesized and introduced to a potential mass aerosol oxidation flow reactor (PAM-OFR) with dry, zero air flowed through a temperature-controlled glass tube to elucidate the uptake rates of α-pinene hydroxy nitrate in the presence of ammonium sulfate seed aerosol. α-pinene hydroxy nitrate uptake kinetics are determined via analysis of hydroxy nitrate concentrations in the gas phase using a high-resolution time-of-flight chemical ionization mass spectrometer (HR-TOF-CIMS). Our results will report on the uptake kinetics of this hydroxy nitrate as a function of relative humidity and seed particle acidity and may provide new insight into the timescales at which α-pinene derived organic nitrates partition to the particle phase, offering more detailed considerations for future modeling studies.

CHAPTER 1: BACKGROUND

1.1 Aerosols

1.1.1 Climate Forcing

A growing concern and hotly debated topic in the public zeitgeist is the anthropogenic impacts to climate change. Greenhouse gases such as CO_2, CH_4, and H_2O, have the most impact on global climate change, contributing approximately 80% of the total radiative forcing from anthropogenic sources (IPCC, AR6). However, as of 2021, the IPCC reports that radiative forcing from aerosol contributes to the most uncertainty in determining the effects of anthropogenic activity on the climate, introducing unpredictability in the fate of atmospheric aerosol and their role in climate change. Figure 1.1 displays the change in effective radiative forcing from 1750 to 2019 as concentrations of different anthropogenic forcing agents have changed from the same time range.
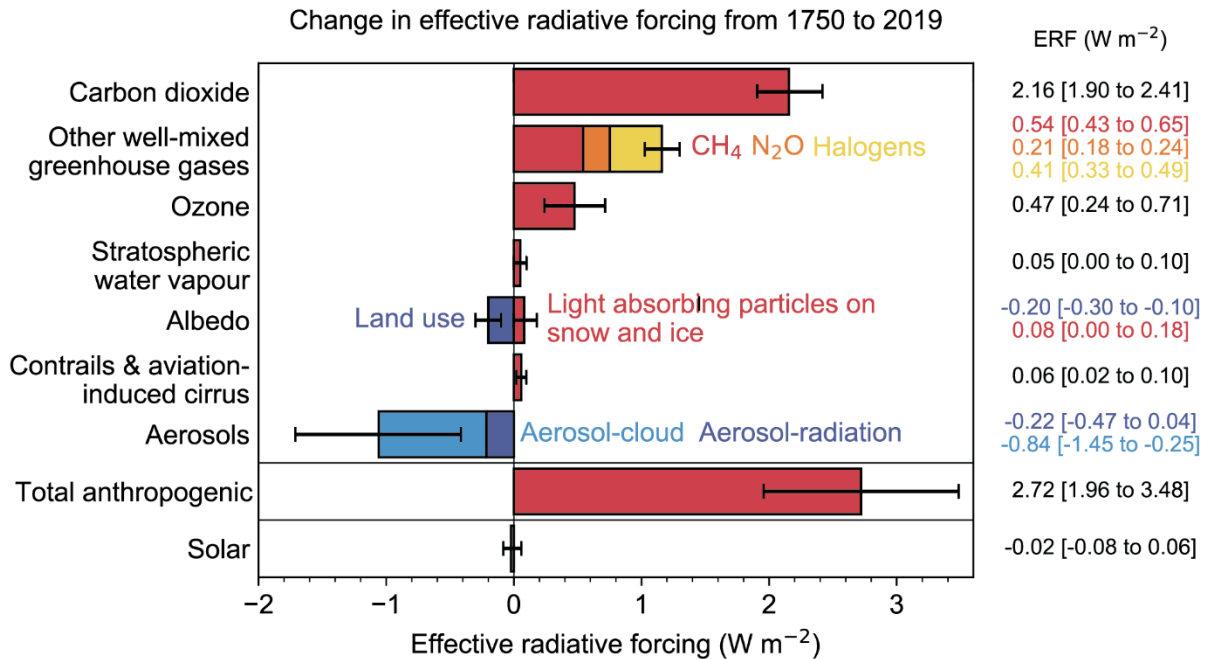
Figure 1.1. Estimates for radiative forcing relative to the pre-industrial era for both gas and particle phase anthropogenic emissions (IPCC, AR6).

Aerosol is defined as solid or liquid particulate matter suspended in gas with size ranges from 0.002 µm – 100 µm in diameter, with the lower end of the diameter range being less defined, due to there being no defined threshold in which a cluster of molecules becomes a particle (Finlayson-Pitts, 2000). Aerosols have both a direct and indirect effect to radiative forcing. The direct effect of aerosols involves the direct absorption or scattering of radiation from the sun. Aerosols emitted from combustion processes such as black carbon can absorb UV radiation and convert this energy to heat, contributing to a net warming effect. Aerosols can also redirect incoming UV radiation from the sun, reflecting the solar radiation away from the Earth's atmosphere and back into space, causing a net cooling effect. Aerosols indirectly affect climate by acting as cloud condensation nuclei where the aerosol has the capability to act as a surface for water to condense onto and nucleate the formation of cloud droplets, encouraging cloud formation and scattering of solar radiation (Twomey et al., 1974). Its impact on the global radiative budget depends on its size, composition, optical properties, and hygroscopicity, which are not fully understood and can change due to chemical and physical aging processes in the atmosphere, e.g., the uptake and growth of condensable organic species.

1.1.2 Health Effects

Aerosols have been closely monitored due to their damaging effects on the respiratory and cardiovascular systems and role in urban pollution. Course particles (<10 micrometers in diameter) originate from primary sources such as direct emission of dust, pollen, sea spray, or combustion. Most harmful, however, are aerosols from the fine (<2 micrometers) and ultrafine (<10 nm) range. Aerosols at this size range can be deposited deep into the lungs (Pinkerton et al., 2000; Raaschou-Nielsen et al., 2013), cause oxidative stress (Dockery et al., 1993; Dockery et

al., 2001; Pope CA 3rd et al., 2004, Harrison and Yin, 2000), and increased mortality (Lester B. Lave & Eugene P. Seskin, 1973; Pope and Dockery, 2006). Once inhaled, aerosol can deposit to the surface of pulmonary bronchiole and alveoli and further pass through to where the respiratory barrier enters the circulatory system, where its components can be absorbed by the bloodstream and spread throughout the body (Xu et al., 2008; Wang et al., 2013). Higher quantities of fine and ultrafine aerosol are deposited in the thoracic cavity in the body compared to coarse particles (Dockery et al., 1993) and accounts for 96% of particles in the gas exchange region of the lungs (Churg and Brauer, 1997). Aerosols in this smaller size range is now more closely associated with health effects and premature death, making fine and ultrafine particles a better indicator for air pollution (WHO, 2006) and necessitates closer monitoring.

1.1.3 Secondary organic aerosol

Fine aerosol in urban zones often scatter light and reduce visibility, creating a "hazy" appearance during high particle concentration days. Fine aerosols mainly originate from secondary sources, whose formation pathways are more complex since they involve multiple series of gas phase reactions and gas-to-particle partitioning of multi-generational products. Secondary organic aerosol (SOA) particles are formed when a parent volatile organic compound (VOC) undergoes oxidation, often with OH, O_3, and NO_3, forming low volatility species that readily partition to the aerosol phase (Kanakidou et al., 2005; Gentner et al., 2012). The products of VOC oxidation can undergo gas-to-particle conversion homogenously through nucleation or heterogeneously by condensation onto existing aerosol (Monks et al., 2009). SOA comprises up to 60% of the total aerosol mass (Chen et al., 2018) and of this, SOA from biogenic sources comprises approximately 58% (Hallquist et al., 2009). With approximately 10,000 to 100,000

3

different organic compounds measured in the atmosphere (Goldstein and Galbally, 2007), it remains difficult to identify the many atmospheric degradation reactions that each compound undergoes. Their subsequent oxidation can then lead to a number of products that may or may not participate in SOA formation, making it a challenge to completely depict all SOA formation mechanisms in the atmosphere.

1.2 (B)VOCs

As discussed above, VOCs are a significant precursor to SOA. VOCs can have both anthropogenic origins as well as natural sources. VOCs from biogenic sources, such as vegetation and foliage, are known as biogenic volatile organic compounds. BVOC contributes ~88% of non-methane VOC emissions, emitted at ~1100 Tg yr^{-1} (Geunther et al., 2012). Isoprene (Figure 1.2) has the highest emission rates of all BVOCs at ~500 Tg yr^{-1} (Geunther et al., 1995; Geunther et al., 2006), making it the most abundant BVOC in the atmosphere. Isoprene contains two double bonds, which are susceptible to attack by oxidants in the atmosphere, making isoprene highly reactive to OH, O_3, and NO_3. Despite this, isoprene has low SOA yields from photooxidation (Kroll et al., 2006; Ng et al., 2008) due to its small size and volatile oxidation products (Carlton et al., 2009) relative to higher carbon number BVOCs such as monoterpenes.
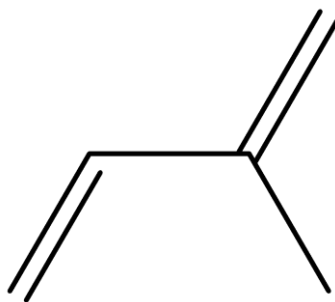
Figure 1.2. Molecular Structure of Isoprene

Monoterpenes ($C_{10}H_{16}$) are a class of compounds that consist of two isoprene (C_5H_8)

units and are commonly emitted from leaves, flowers, and fruits (Alcantara, 2011) as a natural

insecticide (De Moraes et al., 1998). Monoterpenes are emitted at ~157 Tg yr^{-1} (Geunther et al.,

2012), while not as large as isoprene, monoterpene emissions still make significant contributions

to SOA mass loading in the atmosphere. Monoterpenes, like isoprene, are olefinic, making them

highly reactive to the common atmospheric oxidants (OH, O_3, NO_3) and form low-volatility

oxidation products that readily partition to the particle phase (Cahill et al., 2006). Of the

monoterpenes, α-pinene (Figure 1.3) has the highest estimated rate of all monoterpenes (~66 Tg

yr^{-1}) (Geunther et al., 2012) and have high SOA yields (Xu et al., 2015; Rollins et al., 2012).

Relative to isoprene, α-pinene has similar reactivity to OH while having higher reactivity to O_3

and NO_3.
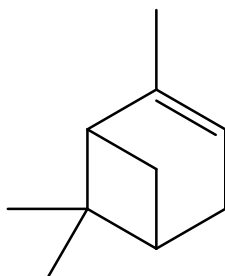
Figure 1.3. Molecular structure of α-pinene

1.3 Atmospheric pollutants

1.3.1 Ozone

Tropospheric ozone is a common oxidant and one of the indicators of atmospheric

pollution. Tropospheric O_3 is of great concern due to its oxidizing nature and its damaging

potential to human health. Elevated and prolonged ozone exposure has been linked to increased

mortality (Mudway and Kelly, 2000) and hospital admissions for pneumonia, chronic obstructive

pulmonary disease, asthma, allergic rhinitis, and other respiratory diseases (Bell et al., 2004; Bell

et al., 2007; Gryparis et al., 2004; Ito et al., 2005). It is estimated that up to 21,000 premature

deaths per year can be associated with excessive, long-term ozone exposure in Europe (EU25,

from WHO paper). Ozone is also damaging to vegetation and agriculture. Ozone exposure can

cause reduced growth and seed production (Wilkinson and Davies, 2009), and visible injury to

leaves and greenery (Manning et al., 2002).

Ozone is generated from the light-initiated oxidation of VOCs in the presence of nitrogen

oxides emitted from industrial processes and the tailpipes of automobiles (EPA) (Eq. 1.1-1.2).

$$NO_2 + hv \rightarrow NO + O \tag{1.1}$$

$$O + O_2 \rightarrow O_3 \tag{1.2}$$

The nitric oxide that is formed from reaction (1) can also react with additional O_3, reforming
NO_2 (1.3):

$$NO + O_3 \rightarrow NO_2 + O_2 \tag{1.3}$$

Once formed, ozone can then photodegrade to form hydroxyl radical, which participates in

countless, rapid photooxidation reactions. Ozone photolyzes to produce oxygen and excited

atomic oxygen (Eq. 1.4). $O(^1D)$ can then react with water vapor to produce two OH radicals (Eq.

1.5):

$$O_3 + hv \rightarrow O_2 + O(^1D) \tag{1.4}$$

$$O(^1D) + H_2O \rightarrow 2OH \tag{1.5}$$

Atmospheric concentrations of OH radical are low and often in the pptv range, however, this is

due to their short atmospheric lifetimes stemming from its high reactivity. OH radical rapidly

reacts with every important species in the atmosphere, and thus is the main determinant of the

oxidation capacity of the Earth's atmosphere (Crutzen et al., 1995).

1.2.3 NO_x

NO_x, which refers to both nitric oxide (NO) and nitrogen dioxide (NO_2), are also of significant interest due to their role in the formation of photochemical smog and tropospheric ozone pollution (Alves et al., 2022). NO_x is mainly anthropogenic in origin, originating from tail pipes from cars and from industrial combustion processes, partitioning from nitric acid, adipic acid, and fertilizer industries (Perez-Ramirez et al., 2003; EU ETS, 2008). NO_x also imposes health risks where upon acute exposure can cause people with existing respiratory conditions to experience respiratory distress and prolonged exposure can damage the respiratory systems (Sousa, 2020). NO_x presents the most risk to public health through its participation in the formation of photochemical smog and ozone production. The main source of tropospheric ozone is the photooxidation of NO_2 (Eq. 1.1-1.2). This often occurs in areas downwind of urban areas with high vehicular emissions or in cities such as Los Angeles where the local topography creates a temperature inversion over the city. The reaction of NO_x with VOCs, which concerns this thesis, also generates SOA particles, creating a brown "haze" that obscures vision during times of high vehicular traffic in cities. This formation begins with the OH radical initiated oxidation of VOCs in the presence of high NO_x (Eq. 1.6). OH radical can add across double bonds or abstract a hydrogen from hydrocarbons, generating a radical that quickly reacts with oxygen to form a peroxy radical ($RO_2\cdot$) (Eq. 1.7).

$$R\text{-}H + OH\cdot \rightarrow R\cdot + H_2O \tag{1.6}$$

$$R\cdot + O_2 \rightarrow RO_2\cdot \tag{1.7}$$

In the presence of NO, the peroxy radical can react to form organic nitrates, or form the alkoxy radical and NO_2, summarized as follows:

$$RO_2\cdot + NO \rightarrow RONO_2 \tag{1.8}$$

$$RO_2\cdot + NO \rightarrow RO\cdot + NO_2 \qquad\qquad (1.9)$$
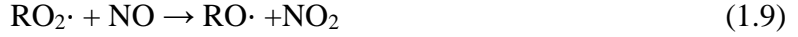
The ratio of the reaction rate of reaction (1.8) and the sum of the reaction rates of 1.8 & 1.9 is the organic nitrate branching ratio. The alkoxy radical (RO·) generated from (1.9) will then react with oxygen to form a carbonyl compound and $HO_2\cdot$. $HO_2\cdot$ reacts with NO to form OH radical and NO_2.

$$RO\cdot + O_2 \rightarrow R_HO + HO_2\cdot \qquad\qquad (1.10)$$

$$HO_2\cdot + NO \rightarrow OH\cdot + NO_2 \qquad\qquad (1.11)$$

The summarized reaction scheme can be seen in Figure 1.4.
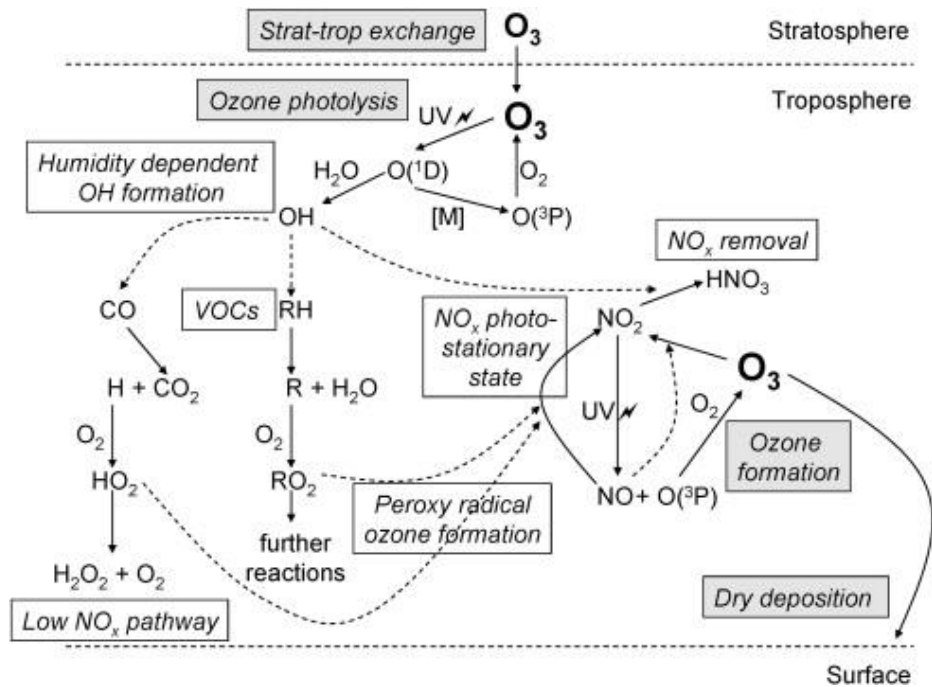
Figure 1.4. Major reaction pathways and sinks for NOx and O3 formation in the lower atmosphere. Adapted from Cape et al., (2008).

This entire reaction scheme regenerates its precursor (OH radical), generates additional NO_2, an O_3 precursor, and generates organic nitrates ($RONO_2$). This is a positive feedback loop, since the regeneration of OH radical means that NO_2, and ultimately O_3, can keep being

produced such that there is still VOC in the air to oxidize. It is important to note that this reaction scheme is most dominant during the day. At night, in the absence of sunlight, NO_3 radical builds up from the oxidation of NO_2 by O_3 because of its short photolytic lifetime during the day (Wayne et al., 1991; Brown and Stutz, 2012). NO_3 radicals will react with BVOCs either through hydrogen abstraction to form HNO_3 or addition across a double bond to form nitrooxy peroxy radicals. The radical will then react to form a closed shell organic nitrate ($RONO_2$). Organic nitrates are low-volatility and readily partition to the aerosol phase, SOA that scatters sunlight and casts a "haze" over cities.

1.2.4 Alpha Pinene Nitrate

The molecule observed in this thesis is an organic nitrate formed from the photooxidation of alpha pinene called alpha pinene hydroxy nitrate (APN). APNs are generated from a series of gas-phase reactions initiated by the atmospheric oxidants O_3, OH, and NO_3 radical. This process starts with reactions (1.12-1.13) with the formation of hydroxyl radical from the O_3 initiated oxidation of NO (1.1-1.2, 1.4-1.5). This generates either APNs (1.14b) or forms an alkoxy radical that oxidizes NO and eventually forms O_3.
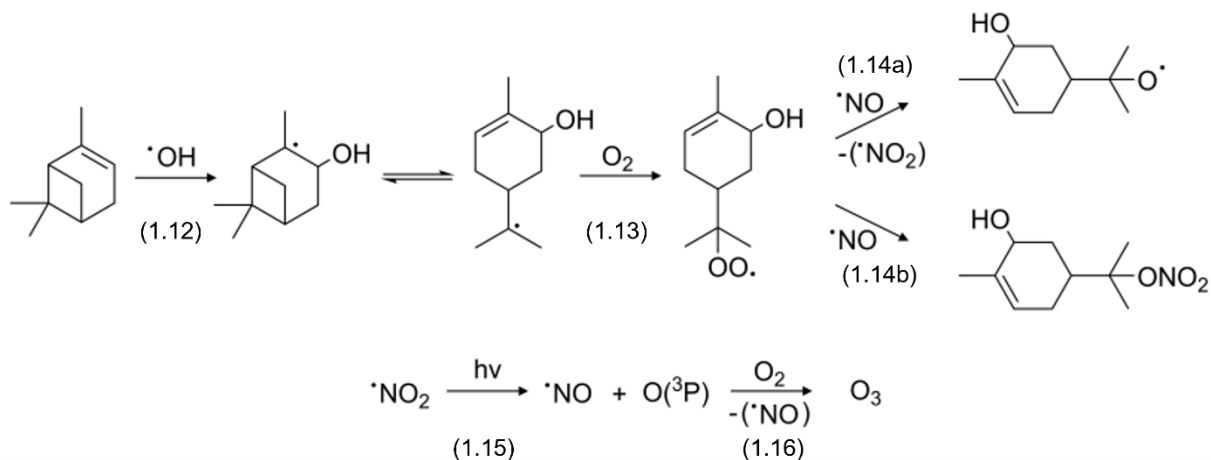
Figure 1.5. Mechanism of the formation pathways for the OH initiated oxidation of alpha pinene to generate alpha pinene nitrate, NO_2, and additional O_3. Adapted from Rindelaub et al., (2016).

The products of the chain termination step (1.14b) are low-volatility and more hydrophilic than the precursor VOC, making them readily partition to the particle phase (Perraud et al., 2012), effectively acting as a reservoir for NO_x and potentially controlling SOA formation (Rollins et al., 2012) and slowing O_3 production (Browne and Cohen, 2012). Previous studies have shown that varying environmental conditions can influence the rates of uptake of APNs onto seed aerosol such as relative humidity and seed aerosol acidity (Liu et al., 2012; Rindelaub et al., 2015; Rindelaub et al., 2016). It is theorized that APNs undergo an acid-catalyzed hydrolysis reaction once in the particle phase (Rindelaub et al., 2015), implying greater uptake and greater loss of the gas-phase APNs that is observed in both laboratory (Nguyen et al., 2011) and field (Day et al., 2010) measurements at increased relative humidity and lower aerosol pH. Despite extensive research, the mechanism for the acid-catalyzed hydrolysis of organic nitrates is still uncertain. At higher pH, the S_N2 mechanism is believed to be the prevalent reaction pathway (Baker and Easty, 1950; Boschan et al., 1955), however, recent literature suggests that a unimolecular reaction mechanism occurs at lower pH and in the presence of water (Rindelaub et al., 2015).

In past work, organic nitrate hydrolysis rates varied greatly between 6.8×10^{-3} s^{-1} (Jacobs et al., 2014) and 1.1×10^{-11} s^{-1} (Darer et al., 2011), contributing to the uncertainty of the fate of organic nitrates both in the gas and particle phases. It is also uncertain whether seed particle acidity changes hydrolysis rates. Chamber and bulk phase analysis have shown varied results, with seed particle acidity being the main influence in increasing rates of hydrolysis (Rindelaub et al., 2016; Morales et al., 2021) as well as seed particle acidity having almost no influence on hydrolysis rates (Darer et al., 2011; Takeuchi and Ng, 2019). Currently, there have been no studies monitoring the APN concentration in the gas phase and observing its loss after the introduction of seed aerosol as all previous studies of APN hydrolysis were performed in the bulk phase, meaning that direct comparison of results will be somewhat impaired by the varying experimental conditions of past experiments. Hydrolysis/uptake rates of APN in this study are expected to be higher than those observed in previous studies, since APNs have a higher molecular weight than other monoterpene derived organic nitrates and are less volatile, meaning they partition to aerosol more readily. In an effort to better understand the impacts of organic nitrate formation on air quality, this study aims to experimentally quantify the uptake kinetics at which the resulting APN in the gas phase partitions to the aerosol phase, specifically as a function of RH and seed particle acidity.

1.3 Research Aims

The goal of this thesis is to better understand the role of RH and seed particle acidity on the reactive uptake kinetics of an alpha pinene-derived hydroxy nitrate onto seed aerosol particles. This has the following aims:

1. Synthesis, purification, and quantification of alpha pinene hydroxy nitrate.

2. Detection and quantification of alpha pinene hydroxy nitrate using chemical ionization mass spectrometry.

3. Calculate uptake rates, uptake coefficients (γ) and mass accommodation coefficients (α) of alpha pinene nitrate uptake onto seed aerosol particles with varying laboratory conditions.

4. Investigate the role of seed aerosol pH and relative humidity on uptake rate, uptake coefficient, and mass accommodation coefficient of the alpha pinene-derived hydroxy nitrate.

CHAPTER 2: EXPERIMENTAL METHODS

Chapter 2. Experimental Methods

2.1 Experimental Set-Up and Conditions

2.1.1 Aerosol Generation

In these experiments, two different seed aerosol conditions were utilized based on the experiments from Rindelaub et al., 2015, Rindelaub et al., 2016, and Surratt et al., 2008. Aerosol was generated using the Constant Output Atomizer (Model 3076, TSI) seen in figure 2.1. Seed particle pH was varied by changing the bulk solution being atomized. Neutral seed was created using a 15 mM solution of $(NH_4)_2SO_4$ (Macron Chemicals, 99%) and acidic seed was created using a mixture of 15 mM $(NH_4)_2SO_4$ and 15 mM H_2SO_4 (Fischer Scientific, 98%). The designation of "neutral seed" in this experiment is still acidic but is named as such for clarity. Sulfate salts for aerosol generation were chosen to mimic atmospheric conditions, as sulfate ion is ubiquitous in the ambient atmosphere in urban environments.
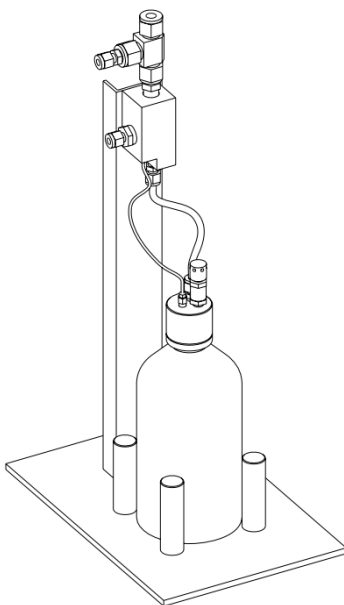
Figure 2.1. Model 3076 constant output atomizer. Figure adapted from TSI instruments.

Using a zero-air generator (Sabio, Model 1001), approximately 20 psi of compressed zero air is flowed into the inlet of the atomizer and forms a high velocity jet. Atomizer solution in the bottle is drawn into the atomizing section through a vertical passage. Large droplets are impacted on the wall opposite to the jet spray and removed while excess liquid is recirculated to the atomizer bottle. A fine aerosol spray flows out at around 1.8 LPM from the top of the block. This process is visualized in the schematic in Figure 2.2.
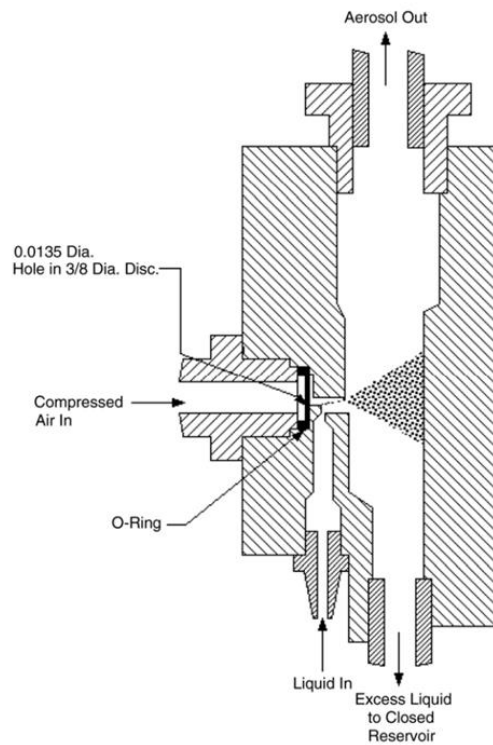
Figure 2.2. Schematic of the atomizing block. Figure adapted from TSI Instruments constant output atomizer manual.

Experiments were conducted at 20-90% RH. For RH lower than 80%, aerosol particles were passed through a diffusion dryer prior to entering the flow tube. The diffusion dryer is a cylindrical wire screen surrounded by silica beads (Figure 2.3). As wet aerosol flow travels through the dryer, the hygroscopic silica beads absorb water vapor and promote the diffusion of

14

water out of the particle stream to "dry" the particles. To achieve >80% RH, aerosol particles bypassed the diffusion dryer and entered directly into the flow reactor.
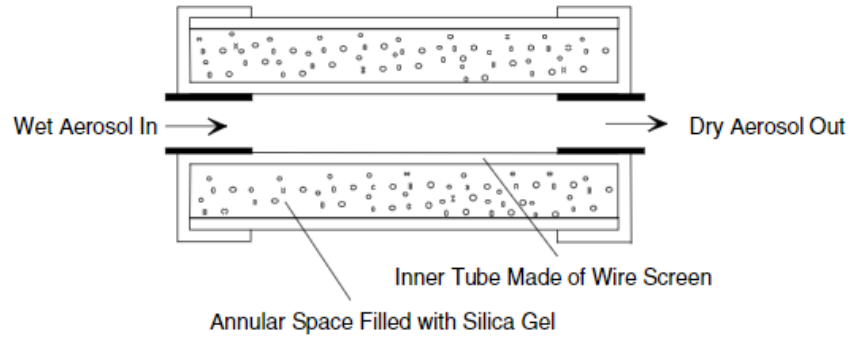
Figure 2.3. Schematic of a diffusion dryer. Figure from TSI Instruments.

2.1.2 Scanning Electrical Mobility Spectrometer

To obtain measurements of particle size distributions and concentrations, a scanning electrical mobility spectrometer (SEMS) (Brechtel, Model 2100) coupled with a mixing condensation particle counter (MCPC) (Brechtel, Model 1720) sampled downstream of the flow tube. Aerosol was sampled at a flow rate of 0.36 LPM and first into a Po-210 neutralizer to remove static charges on the particles, yielding an equilibrium distribution of positive charges on the particles. The aerosol flow was then sampled into a differential mobility analyzer (DMA) shown in figure 2.4. The DMA records size distributions by separating particles based on their particle electrical mobility (Z_p ($m^2V^{-1}s^{-1}$), given by eq. 2.1 (Knutson and Whitby, 1975).

$$Z_p = \frac{\left(Q_p + Q_a\right)\ln(\frac{R_2}{R_1})}{2\pi LV} \tag{2.1}$$

Where Q_p is the sheath flow rate, Q_a is polydisperse flow rate, R1 and R_2 are the radii of the inner and outer electrodes, L is the effective electrode length, and V is the applied voltage.

15

The DMA consists of two concentric metal rods where the outer rod maintains a consistent voltage and the inner rod has a range of voltages to establish an electric field between the two rods. Polydisperse aerosol and sheath air flow between these two rods where the electric field causes positively charged particles to be attracted to the collector rod. Where on the collecting rod the particles settle depends on their particle electrical mobility diameter, which is related to the particle diameter by using Stoke's law (eq. 2.2).

$$d_p = \frac{neC_c}{3\pi\mu Z_p}$$
(2. 2)

Where n is the number of elementary charge units, e is the elementary unit of charge (1.61×10^{-19} C), C_c is the Cunningham slip correction factor, and μ is the gas viscosity. C_c is a function of the aerosol's Knudsen number (K_n) given by eq 2.4 and is related to C_c by eq 2.4.

$$K_n = 2\lambda/d_p$$
(2. 3)

$$C_c = 1 + K_n[1.257 + 0.4\exp(-1.0K_n)]$$
(2. 4)

Particles with a narrow range of Z_p exit through an opening at the bottom of the collector rod, hence, only particles of a specific Z_p leave the DMA. Different sizes can be isolated by changing the voltage of the inner diode, allowing the user to obtain a size distribution of aerosol.
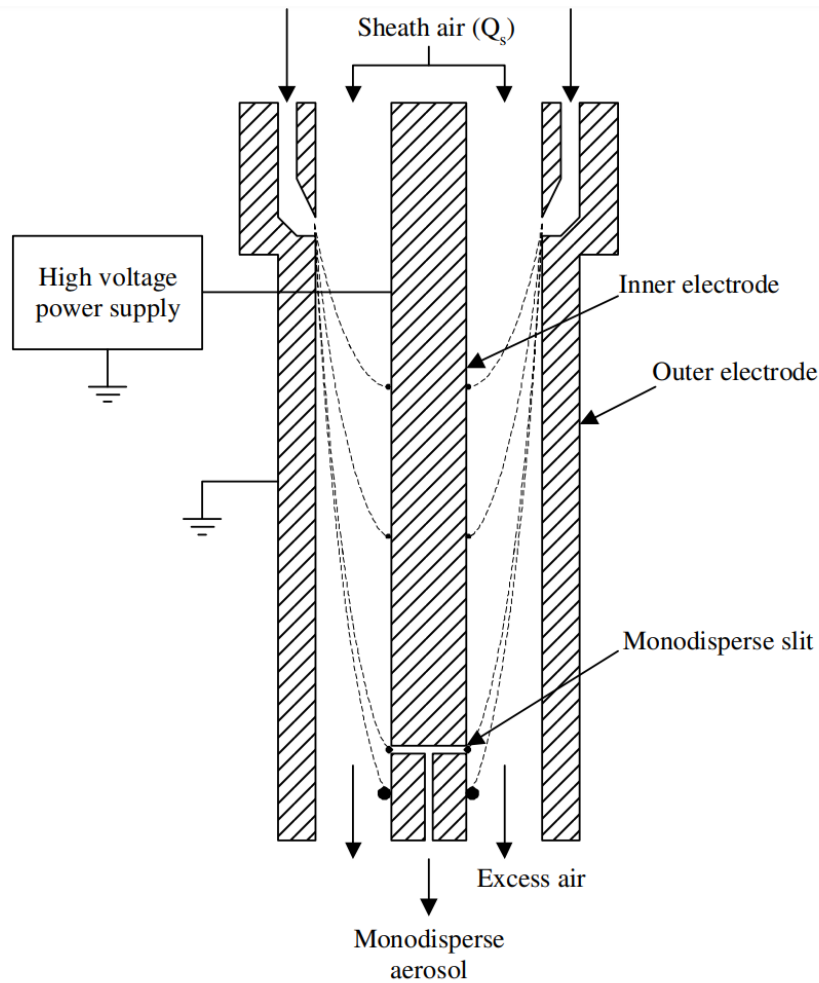
Figure 2.4. Schematic of a differential mobility analyzer. Figure from Intra and Tippayawong, 2008.

After size selection through the DMA, the monodisperse flow of aerosol is sampled in the MCPC (Figure 2.5) to measure particle number concentration. Aerosol entering the MCPC is passed through vaporized butanol and cooled, which condenses butanol onto the surface of the aerosol. This action allows the aerosol to grow to a size that is optically detectable. The aerosol flow is then directed across a laser in which the particles will scatter the applied light. A detector records how many times this applied light is scattered, translating to a count of how many particles pass this light. The number of times a particle passes the laser (n) over a certain time

period (t_p) is then related to particle concentration by equation 2.5 where Q is the sample flow rate.

$$N = \frac{n}{Qt_p} \qquad\qquad (2.5)$$
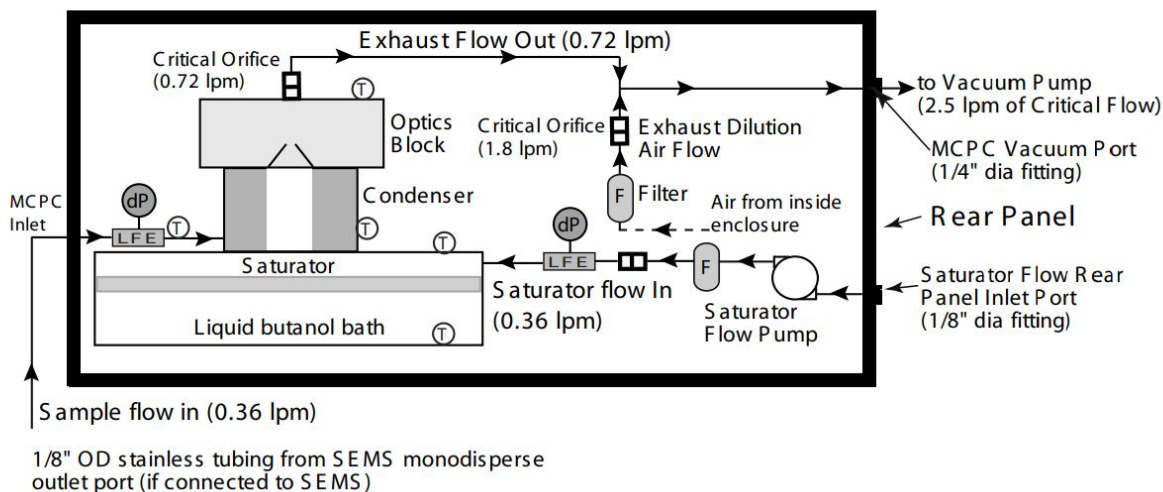
Figure 2.5. Schematic diagram of the CPC. Figure from Brechtel.

2.1.3 High Resolution Time of Flight Iodide Adduct Chemical Ionization Mass Spectrometer

Measurements of APN were taken using a high-resolution time-of-flight chemical-ionization mass spectrometer (HR-TOF-CIMS) (Aerodyne). Chemical ionization was chosen for this technique due to simple sample preparation, high sensitivity, and high-resolution measurement of gas phase compounds (Aljawhary et al., 2013; Bertram et al., 2011; Dougherty et al., 1975; Tannenbaum et al., 1975). Chemical ionization of the target molecule proceeds through ion-molecule reactions, in which the reagent ion forms an adduct with the target molecule, seen in Eq 2.6. This soft ionization scheme is ideal for gas phase measurement due to its minimal fragmentation which maintains the parent molecules' structure and composition. In

this experiment, the reagent ion utilized is iodide (from methyl iodide) because of its sensitivity to detecting hydroxy nitrate compounds (Lee et al., 2014).

$$I^- + M \rightarrow M - I^- \tag{2.6}$$

The CIMS consists of five different stages each equipped with a pump, as seen in Figure 2.6. First, sample flow is introduced to the ion-molecule reaction chamber (IMR) through a critical orifice at 2.0 L min^{-1}. The IMR chamber (S1) is equipped with a dry scroll pump (Agilent) that evacuates the chamber to approximately 100 mbar and has a temperature regulator to maintain the IMR at 60 °C. 1 ppm methyl iodide from a cylinder (Linde) is directed orthogonal to the sample flow after passing through a Po-210 radioactive source. After ionization in the IMR, the analyte passes through the first stage (S2), which is held at 2 mbar, and enters the second stage (S3), which is maintained at 0.01 mbar. Two quadrupoles guide the ions through the stages and provide collisional cooling of the analyte, and thus, make the ions energetically homogenous while entering the third stage (S4). Here, the ions are further focused and are orthogonally pulsed into the time-of-flight (TOF) analyzer, where ions are separated by their mass based on their arrival time to the detector.
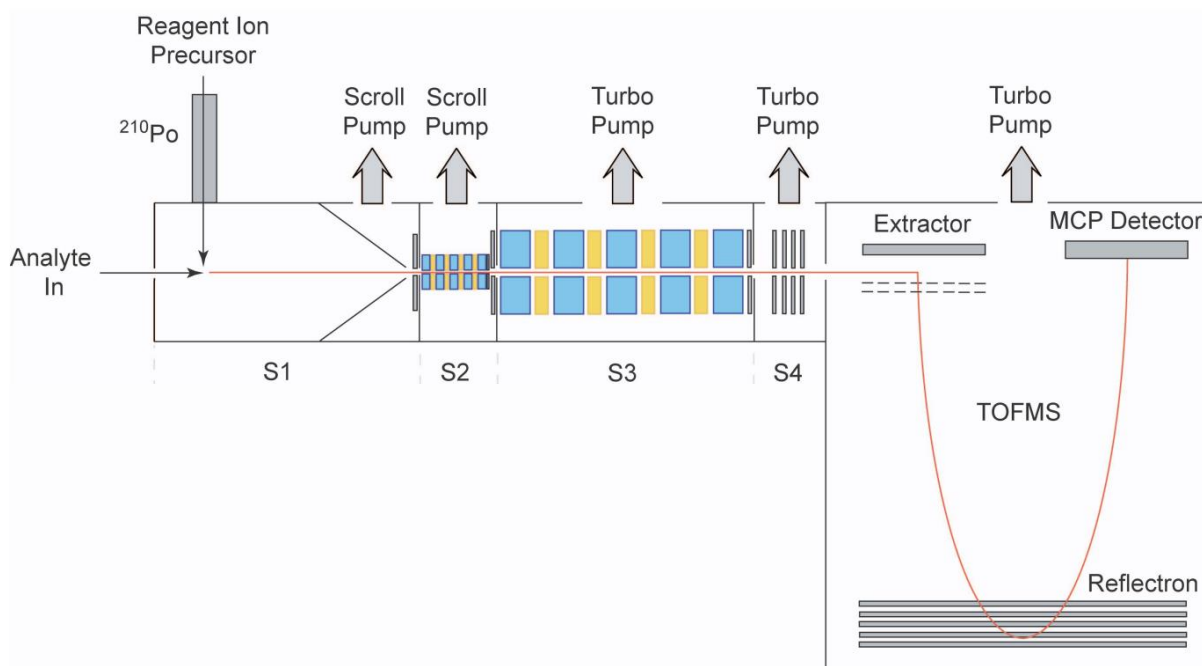
Figure 2.6. Schematic diagram of the HR-TOF-CIMS. Adapted from Bertram et al., 2011

2.1.3.1 Effect of RH on APN Signal

It has been shown that relative humidity of sample flow into the CIMS influences the

sensitivity of the instrument (Kercher et al., 2009; Slusher et al., 2004). APN and water compete

with the iodide ion, thus, the additional presence of water forms water-iodide clusters, leaving

less iodide to ionize and form adducts with APN, i.e., lowering the sensitivity for iodide-adduct

CIMS with APN (Lee et al., 2014). To circumvent any changes in sensitivity due to water vapor,

0.1 LPM of humidified air was flowed into the IMR inlet, seen in Figure 2.8 and 2.9. However,

changes in sensitivity were still observed and the APN signal would decrease with increasing

relative humidity. To correct and quantify the changes in sensitivity, a calibration curve was

generated, seen in Figure 2.7. The slope of this calibration curve was utilized if any changes in

RH were observed during the experiment.
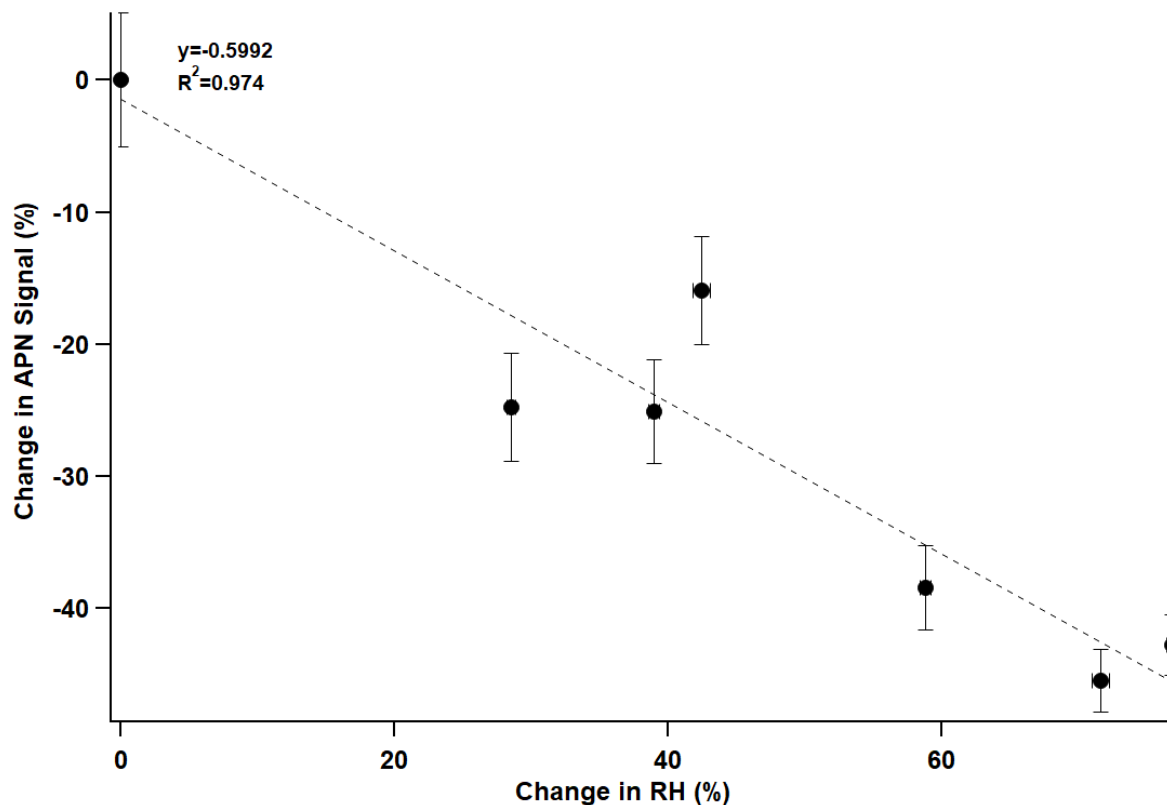
Figure 2.7. Calibration curve for APN signal change with changing RH.

2.1.4 Extractive Electrospray Ionization Time-of-Flight Mass Spectrometer

Measurement of aerosol composition was performed using an extractive electrospray ionization time-of-flight mass spectrometer (EESI-TOF) (Aerodyne). The EESI-TOF provides online measurements using a soft ionization method, leading to minimal fragmentation and maintaining the molecular formula (Lopez-Hilfiker et al., 2019). The EESI-TOF is an extractive electrospray inlet coupled to commercially available time-of-flight mass spectrometers. Aerosol enters the EESI inlet and passes through a charcoal denuder where gas-phase constituents are assumed to be scrubbed from the aerosol flow. The particles then collide with electrospray droplets and the soluble species in the aerosol are extracted. The droplets pass through a heated capillary to evaporate excess electrospray. Solvent evaporation moves the charged species closer

together due to droplet shrinkage, eventually, the surface tension of the droplet is no longer able to sustain the Coulombic force of repulsion, and the droplet splits through Coulombic explosion. The ionized species then travel to the TOF mass analyzer for measurement.
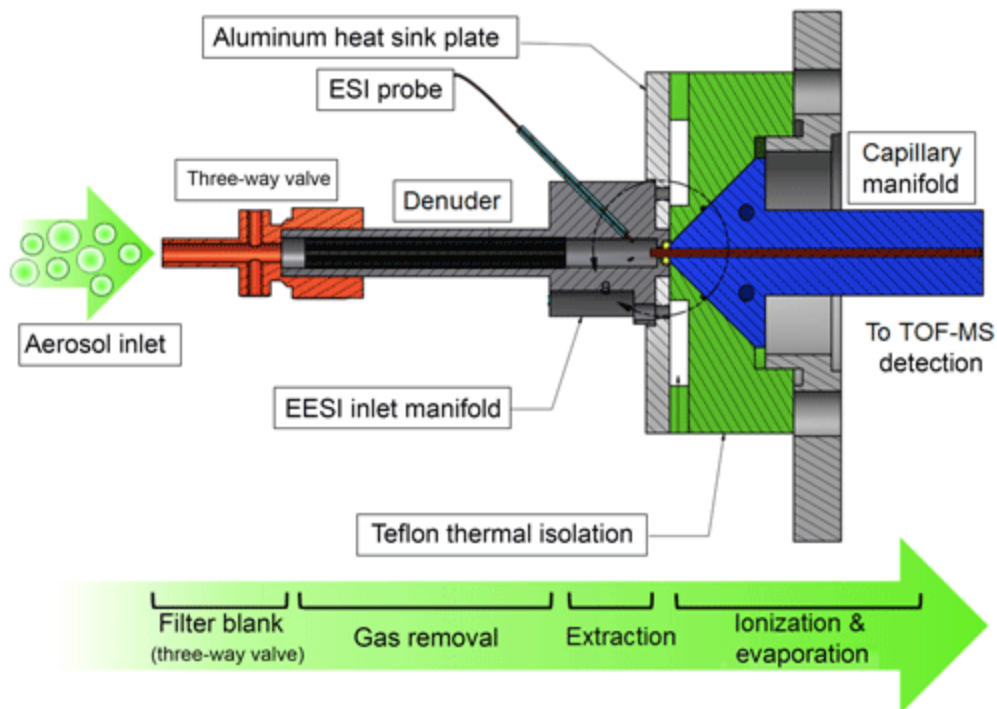
Figure 2.8. Schematic diagram of the EESI-TOF inlet and ionization source. From Lopez Hilfiker et al., 2019.

2.1.5 Flow Tube Experiments

The kinetics of APN uptake onto seed aerosol was assessed by continuous APN flow into the potential mass aerosol oxidation flow reactor (PAM-OFR; Aerodyne Research Inc.) in the presence of aerosol and observing the changes in gas phase APN as a function of residence time or aerosol surface area. The PAM-OFR is a 13.3 L brass chamber equipped with a syringe pump, temperature and RH probes, and lamps to simulate photooxidative aging in the atmosphere (Lambe et al., 2011). As these experiments did not simulate photooxidation, the lamps within the PAM-OFR were off. A programable syringe pump was used to deliver a specified, constant

output of APN into the PAM-OFR. Temperature (± 0.2 °C) and RH (± 2%) sensors were installed to record the conditions in the PAM-OFR.

Additional studies were performed whereby semi-volatile APN was introduced to the flow tube by flowing ~3 LPM of dry, hydrocarbon free, zero air over the liquid APN in a glass vacuum trap. High RH air was introduced by flowing 3 LPM of zero air into a water bubbler containing ultra-pure water and was flowed over the APN and into the PAM-OFR. Note that some undetermined amount of APN in the solution could have reacted with water that partitioned into the solution. This is not expected to affect the uptake kinetics measurement as the kinetics were derived from the difference in the initial APN signal intensity (before addition of aerosol) and final APN signal intensity (in the presence of aerosol).

The change of APN signal in response to the introduction of aerosol was measured using the HR-TOF-CIMS. First, no reactants were introduced to the chamber and a total of approximately 5 LPM of air was flowed through the flow tube to achieve a stable RH and record a blank (background) on the mass spectrometer. Once a stable blank was measured, air was flowed over the APN and the APN signal was allowed to stabilize. Aerosol was then introduced, and the APN signal intensity was monitored as it decreased in response to its uptake by aerosol. APN and aerosol were mixed in the PAM-OFR over the determined residence time of ~3 min, although longer timescales (~30 min) were used for monitoring changes in the APN signal with the HR-TOF-CIMS to allow for equilibration as the aerosol and APN partition to the walls of the PAM-OFR and sample tubing (heated to ~50°C). The aerosol flow was then bypassed, and the APN signal was given enough time to stabilize back to its initial value. This procedure was repeated two more times to obtain a total of three trials per experiment. The experiment was conducted at three different seed particle acidities in both wet and dry conditions. A summary of

experiments conducted can be seen in Table 2.1 with pH of the seed particles estimated using the

Extended Aerosol Inorganics Model (E-AIM) (Clegg et al., 1998). The entire schematic of the

experimental set-up for both high and low RH experiments are represented in Figures 2.9 & 2.10.
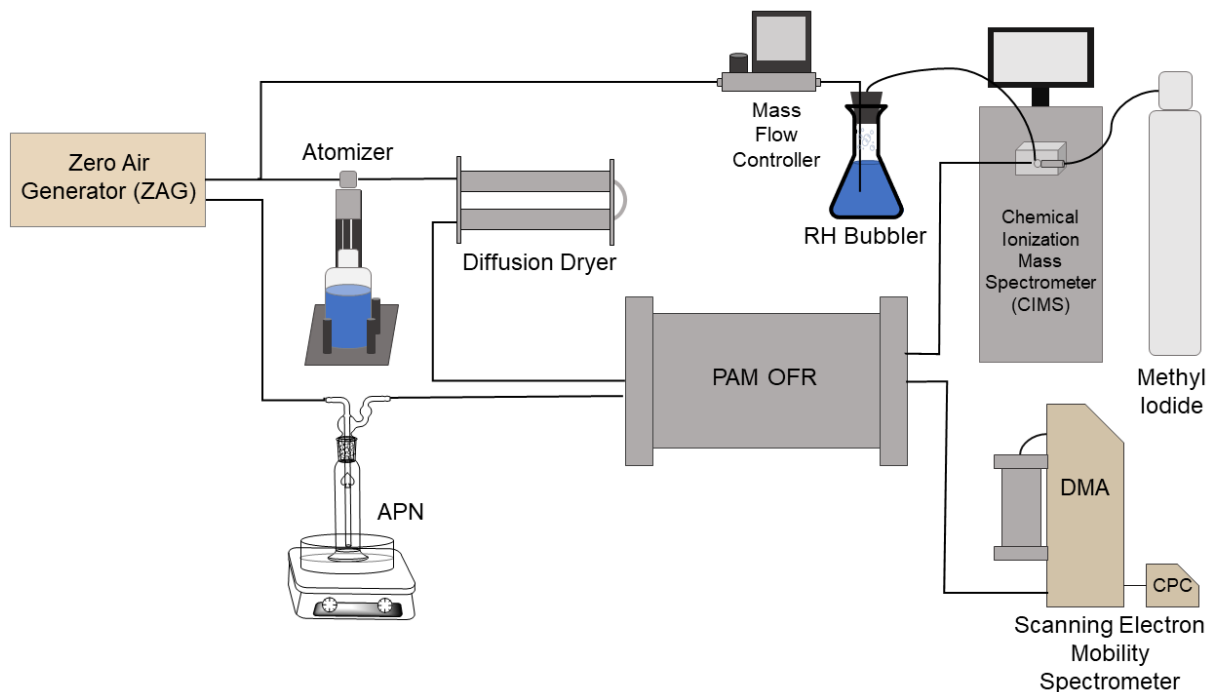
Figure 2.9. Experimental set-up for dry experiments.
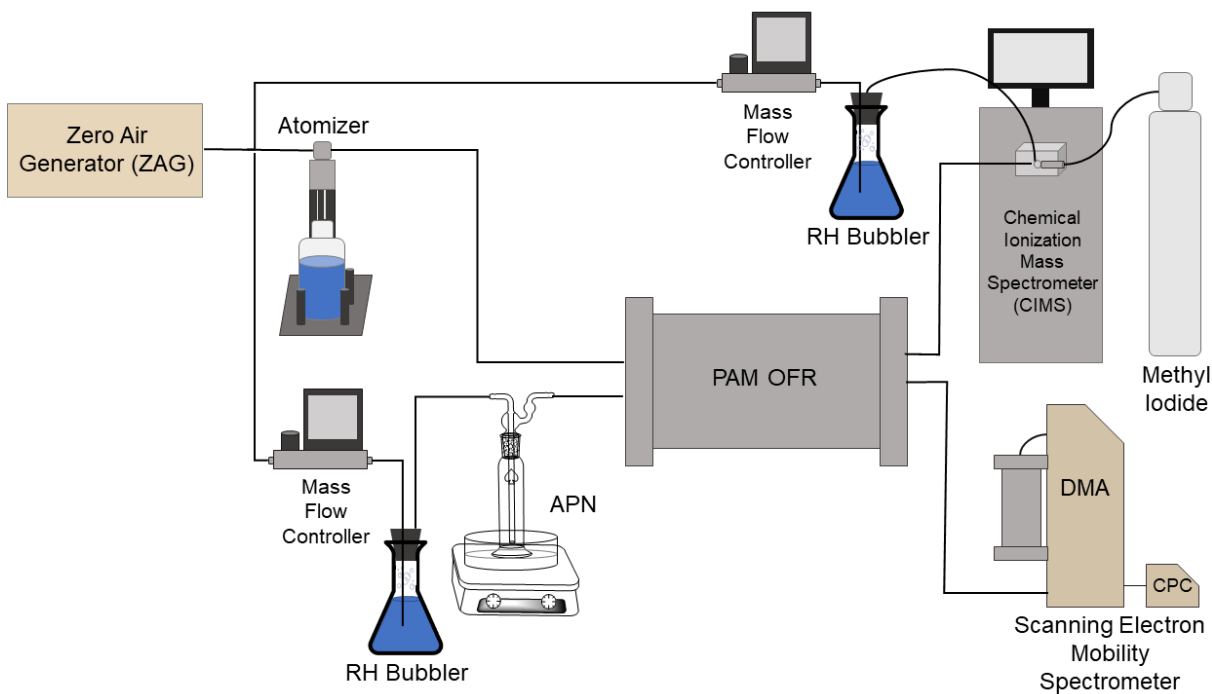
Figure 2.10. Experimental set-up for high RH experiments.

Table 2.1. Summary of experimental conditions from APN uptake experiments.

Particle Seed Acidity	Relative Humidity
1. Acidic Seed (pH ≈ 0.1)	High RH (~90%)
2. Acidic Seed	Mid RH (~70%)
3. Neutral Seed (pH ≈ 4.53)	High RH (~90%)
4. Neutral Seed	Mid RH (~70%)
5. Neutral Seed	Low RH (~20%)

2.2 Calculations

The goal of this thesis is to quantify the kinetic parameters of gas phase uptake of APN onto seed particles and to observe how seed particle acidity and relative humidity affect the kinetics of this interaction. Uptake rates, reactive uptake coefficient, and mass accommodation coefficient for all experimental conditions were calculated to better understand the time scales and extent at which APN heterogeneously reacts with aerosol in the atmosphere.

Uptake rates were calculated by assuming pseudo-first-order loss, seen in the rate equation (eq. 2.7) (Jefferson et al., 1997).

$$\frac{d[APN]}{dt} = -K[APN]_g \qquad (2.7)$$

Where $K=k_1+k_{d,w}$, which is the sum of the loss processes due to pseudo-first order uptake (k_1) and the loss from diffusion and wall loss ($k_{d,w}$). Rate coefficients (K) were calculated by plotting the natural logarithm of the observed loss of APN, i.e $\ln([APN]/[APN]_0)$, as a function of residence time, in which the slope of this plot represents the observed first-order loss rate of APN. K was then corrected with wall loss and diffusion rate ($k_{d,w}$), which was independently

measured in a different experiment, leaving k_1, which represents the first-order loss rate of APN due to uptake onto the aerosol with corrections for wall loss. For first order reactions, reactive uptake (γ) can be calculated using equation 2.8, as described in Fuchs et al., 1971, Kroll et al., 2015, and George and Abbatt, 2010.

$$\gamma = \frac{4k_1}{\omega S_a} \tag{2.8}$$

Where ω is the mean molecular speed of gas phase APN in cm s^{-1} and S_a is the total surface area concentration in cm^2 cm^{-3}.

Gas uptake onto polydisperse aerosol can be described in terms of mass accommodation (α) using the approach described in Fuchs-Sutugin 1970, as seen in Equation 2.9.

$$k_1 = \sum_i \frac{\alpha N_p \omega \pi D_{p,i}{}^2 \frac{dN}{dlogD_{p,i}}}{4(1 + \alpha\beta)} \Delta logD_{p,i} \tag{2.9}$$

$$\beta = \frac{(0.76 + 0.283K_n)}{K_n(K_n + 1)}$$

$$K_n = \frac{6D_g}{\omega D_p}$$

Where N_p is the particle number density in particles cm^{-3}, D_p is the mean particle diameter in cm, K_n is the Knudsen number, D_g is the gas-phase diffusivity constant, β is the diffusive resistance term. α was iteratively calculated such that the calculated k_1 is equal to the experimentally determined k_1.

2.3 Synthesis, Purification, and Quantification of α-Pinene Hydroxy Nitrate

2.3.1 Synthesis

A standard for mass spectrometric analysis was required to quantify the kinetic parameters of α-pinene hydroxy nitrate (APN) uptake onto aerosol particles. Since APNs are not commercially available, APN was synthesized according to Pinto et al., (2007) with adjustments based on the nitration of alpha-pinene oxide. Approximately 0.33 g of bismuth (III) nitrate pentahydrate ($Bi_3(NO_3)_3 \cdot 5H_2O$) (Sigma Aldrich, ~96%) was added to a 50 mL round bottom flask with approximately 10 mL dichloromethane (DCM) (Fischer, 99.9%). With gentle stirring, approximately 0.1 g of α-pinene oxide (Sigma Aldrich, 97%) was added dropwise with a syringe through a rubber septum. The reaction setup is visualized in Figure 2.11. The reaction was stirred for approximately 1 hour. After 1 hour, product was spotted on an aluminum-backed TLC plate and allowed to develop in 80:20 hexanes to ethyl acetate solvent to confirm reaction completion. The desired product has an approximate R_f value of 0.3 (McKnight et al., 2012). DCM was then evaporated using a rotary evaporator (BUCHI, Model R-100) until only a clear, oily product remained.
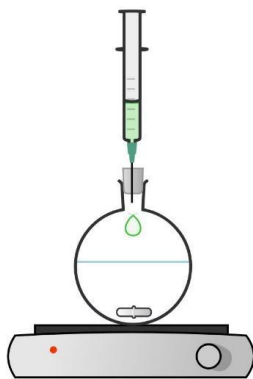
Figure 2.11. Reaction set-up for APN synthesis.
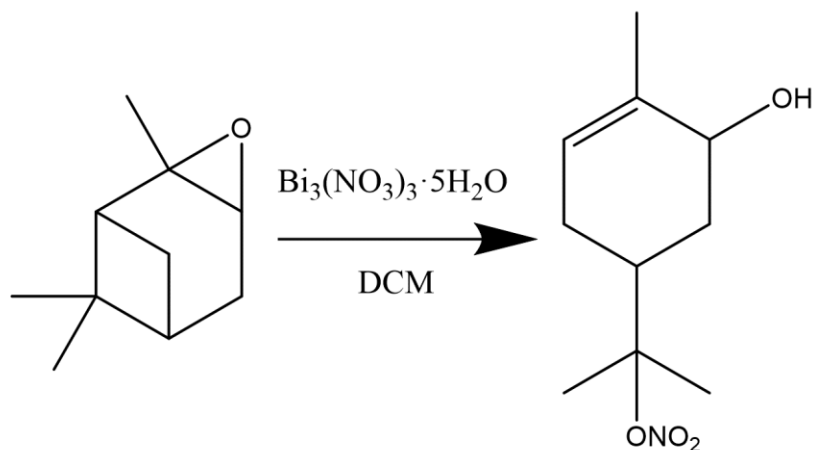
Figure 2.12. Theorized chemical reaction utilized for synthesis of APN.

2.3.2 Purification

Purification of crude APN was performed using flash chromatography. A liquid chromatography column was packed first with cotton, then sand, and with ~15 cm silica gel slurry made with 80% hexanes (Fischer Chemicals, 99.5%) and 20% ethyl acetate (Honeywell, 99.9%). The liquid chromatography column was filled entirely with solvent and left to run through the silica gel. Raw APN was then carefully added to the top of the stationary phase and allowed to run into the silica gel until mobile phase was added. The liquid chromatography column was then fitted with a vacuum adapter to perform flash chromatography. Separation was performed under ultra-high purity nitrogen (UHP N_2) to discourage oxidation of the raw APN and to accelerate the purification. Approximately 40 fractions of approximately 15 mL were taken, and each fraction was spotted on a TLC and developed to elucidate the fractions that contained the desired product. The purified APN consistently separated in fractions 33-38, and multiple fractions with the same product were combined and evaporated until only a clear oily product remained.

2.3.3 Identification

2.3.3.1 TLC Silica Gel Separation Analysis

The required time for the completion of the APN synthesis was determined empirically with thin-layer chromatography (TLC). The polar stationary phase is silica gel adhered to an aluminum sheet (Millipore Sigma, 200μm silica gel thickness) and the mobile phase was a 20% ethyl acetate and 80% hexane mixture. After one hour of stirring, approximately 0.5 μL of the reaction mixture was taken and spotted onto the TLC plate. The TLC plate was then allowed to develop in a developing chamber until solvent had climbed to an appropriate height on the TLC plate (~ 6cm). Once the TLC plate was finished developing, it was dipped in $KMnO_4$ to oxidize the spots to a yellow color, leaving the rest of the plate stained purple. The starting material and reaction mixture were both spotted and developed, seen in Figure 2.12. The starting material has very faint spots, with spots of the same R_f appearing much stronger in the product. As stated earlier, desired product has an R_f of ~0.3, which is the circled spot on the right plate, implying that the reaction had generated APN. The appearance of the same spots as those in the unreacted starting material implies the reaction was not completed. To investigate this, the reaction was allowed to stir for an additional hour and spotted again for TLC analysis. Results remained the same, however, with unreacted starting material remaining in the product. This was then remediated by subsequent purification of the crude material.
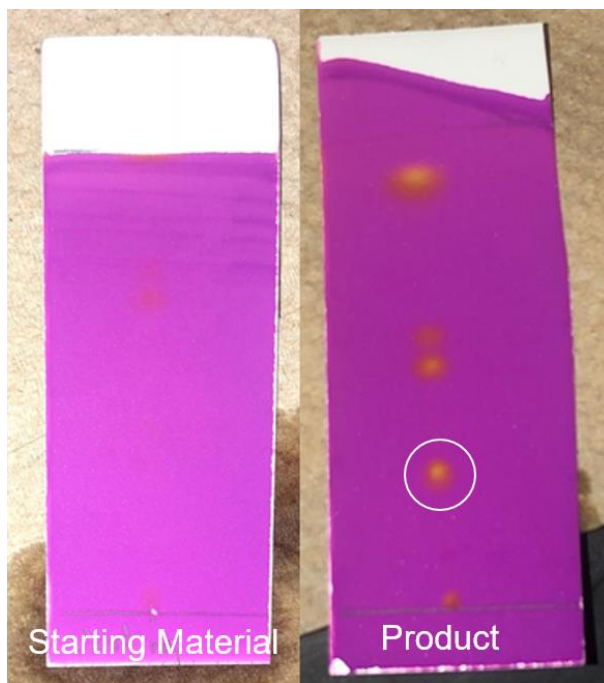
Figure 2.13. TLC Plate Separation of the unreacted starting material (left) and the synthesized product (right).

2.3.3.2 NMR Analysis

Structural information of the synthesized APN was further elucidated using ^{1}H NMR analysis. To prepare the purified sample for NMR analysis, all solvent from the collected fractions from flash chromatography would be evaporated, leaving ~1 mL of sample. To this, ~1 mL of deuterated chloroform (Cambridge Isotope Laboratories, 998%) was added to the same vial.
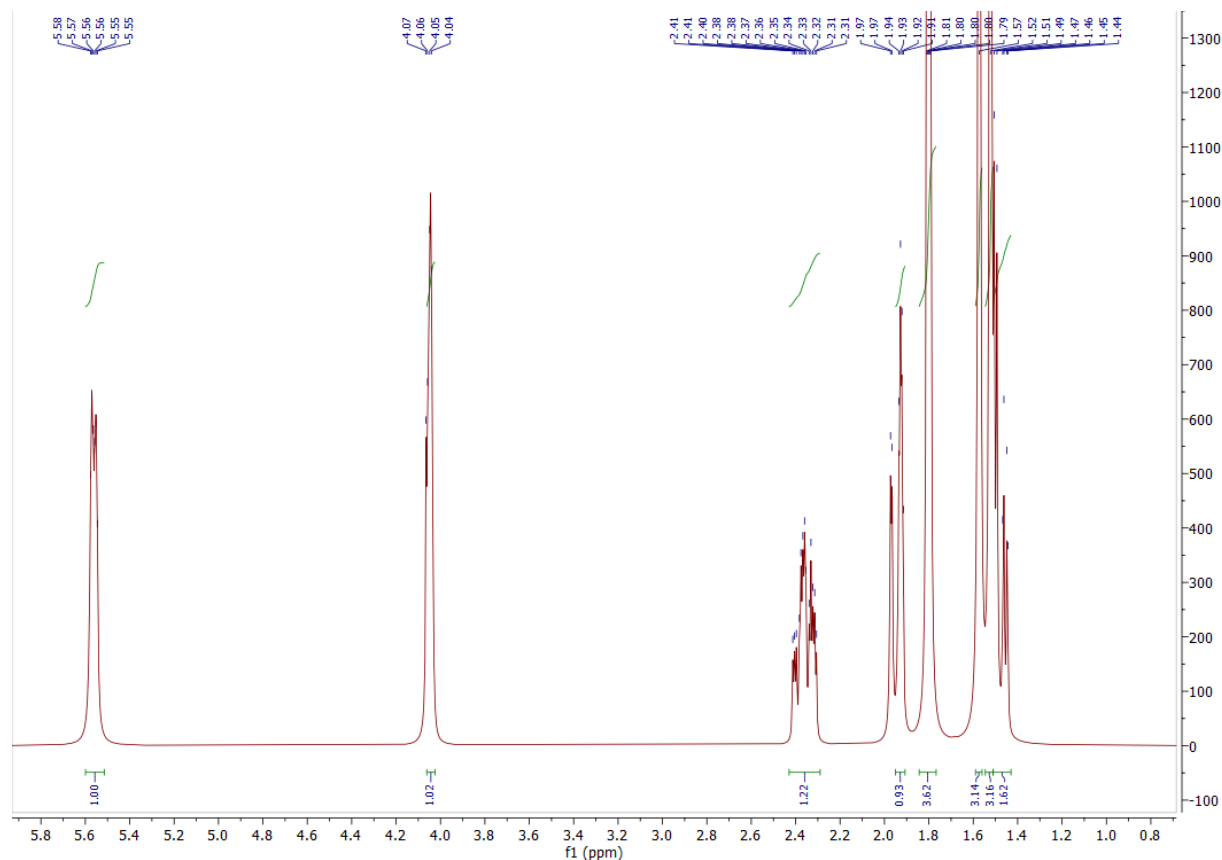
Figure 2.14. ^{1}H NMR spectrum of the purified, synthesized sample of APN.

The chemical shifts, peak multiplicities, and integrations from the ^{1}H NMR spectrum are as

follows: δ 5.56 (m, 1H), δ 4.05 (t, 1H), δ 2.40 (m, 1H), δ 1.94 (t, 1H), δ1.80 (S, 3H), δ1.57 (s,

3H), δ1.52 (s, 3H). The APN has protons that include complicated splitting patterns, impeding

the definite peak assignments using figure 2.13. Rather than utilizing the ^{1}H NMR spectra to

elucidate a specific structure, it was utilized in this case to confirm the presence of the APN.

The two methyl groups at δ 1.57 and δ1.52 are downshifted, suggesting shifts due to proximity to

a nitrate group. The multiplet at δ5.56 is also characteristic of a vinyl hydrogen, implying the

presence of a double bond within the molecule. While this is not sufficient to completely resolve

the structure of the synthesized sample, the same 1H NMR pattern was observed and confirmed

with 13C NMR as in Rindelaub et al., 2016 (shown in their supplementary material). Therefore,

31

it is assumed that the tertiary nitrate APN was synthesized. The presence of APN was confirmed here due to the combination of TLC, ^{1}H NMR, and mass spectrometric analysis.

2.3.4 Quantification

Alpha pinene hydroxy nitrate quantification was achieved using quantitative H^1 NMR analysis using the method described in Barti et al., 2012. Product was weighed and ~1g of deuterated chloroform and ~ 2 µL of benzene was added to prepare for quantitative NMR analysis. The molar ratio between APN and benzene was determined using the following relationship:

$$\frac{M_x}{M_y} = \frac{I_x}{I_y} \times \frac{N_x}{N_y}$$ (2. 10)

Where *x* refers to APN, *y* refers to benzene, M_x/M_y is the molar ratio between APN and benzene, *I* is the integral area of the corresponding peak, and *N* is the number of nuclei. Using the relationship in eq 2.10, the concentration of APN was calculated for a specific sample. The solution concentration was typically 1.4×10^{-2} M $\pm$ 5.6×10^{-3}M.

After purification and NMR analysis, a calibration curve was generated with the mass spectrometer. Using the syringe pump equipped on the PAM-OFR, a known quantity of APN was injected at known rates to elucidate mass concentrations of APN in the PAM-OFR. To vary the concentrations of APN being sampled by the mass spectrometer, the syringe pump was programmed to inject the sample at different rates. As different concentrations were injected into the PAM-OFR, the signal response from the CIMS was recorded. The calibration curve for this process can be seen in Fig. 2.15.

$$y=0.60952+4.1592$$
$$R^2=0.972$$
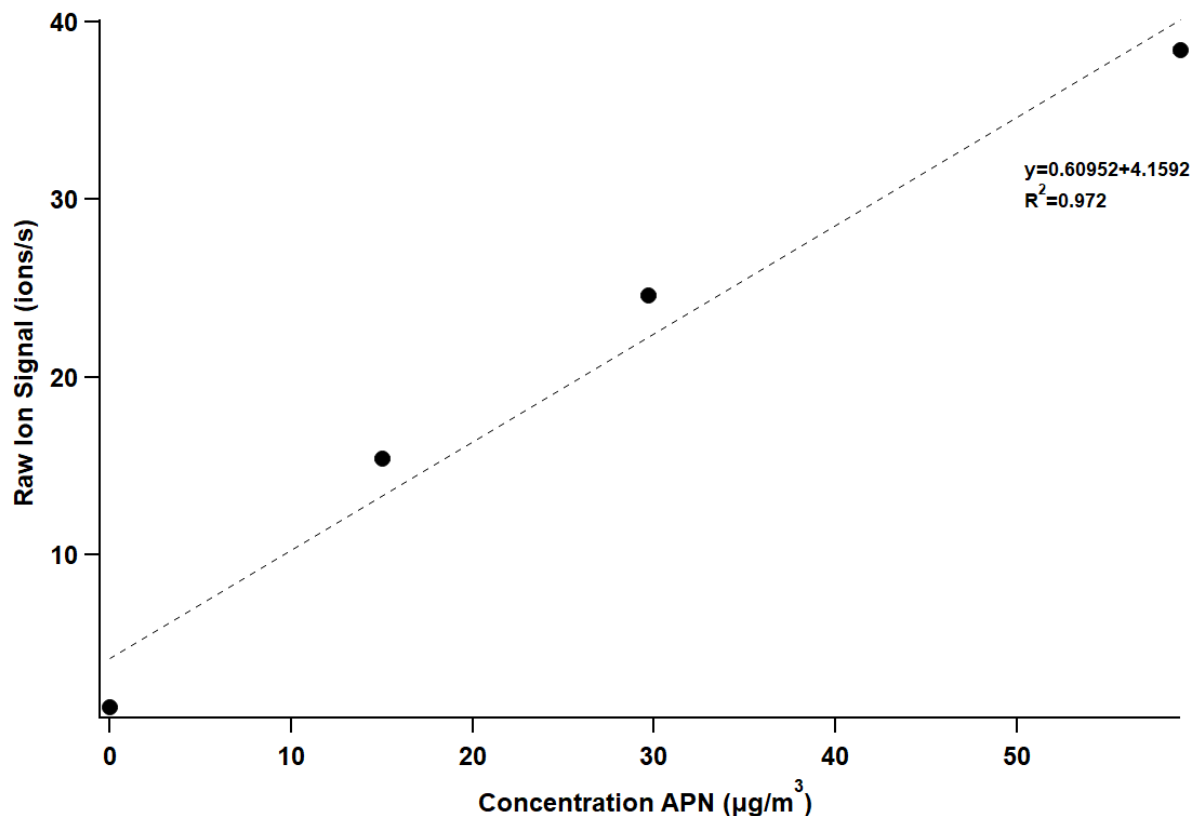
Figure 2.15. Example calibration curve for APN using the high-resolution time-of-flight chemical ionization mass spectrometer.

2.4 APN detection by CIMS

APN loss rates were determined using the relative signal loss of APN in the presence of aerosol, measured by iodide-adduct CIMS. Figure 2.16 shows the average mass spectrum of gas phase species of the background (zero air; dashed gray line), following APN injection (black), and APN in the presence of aerosol (green). The mass spectra in Fig. 3.1 were from experiment 5 in Table 2.1, i.e., neutral seed particle and low chamber RH.
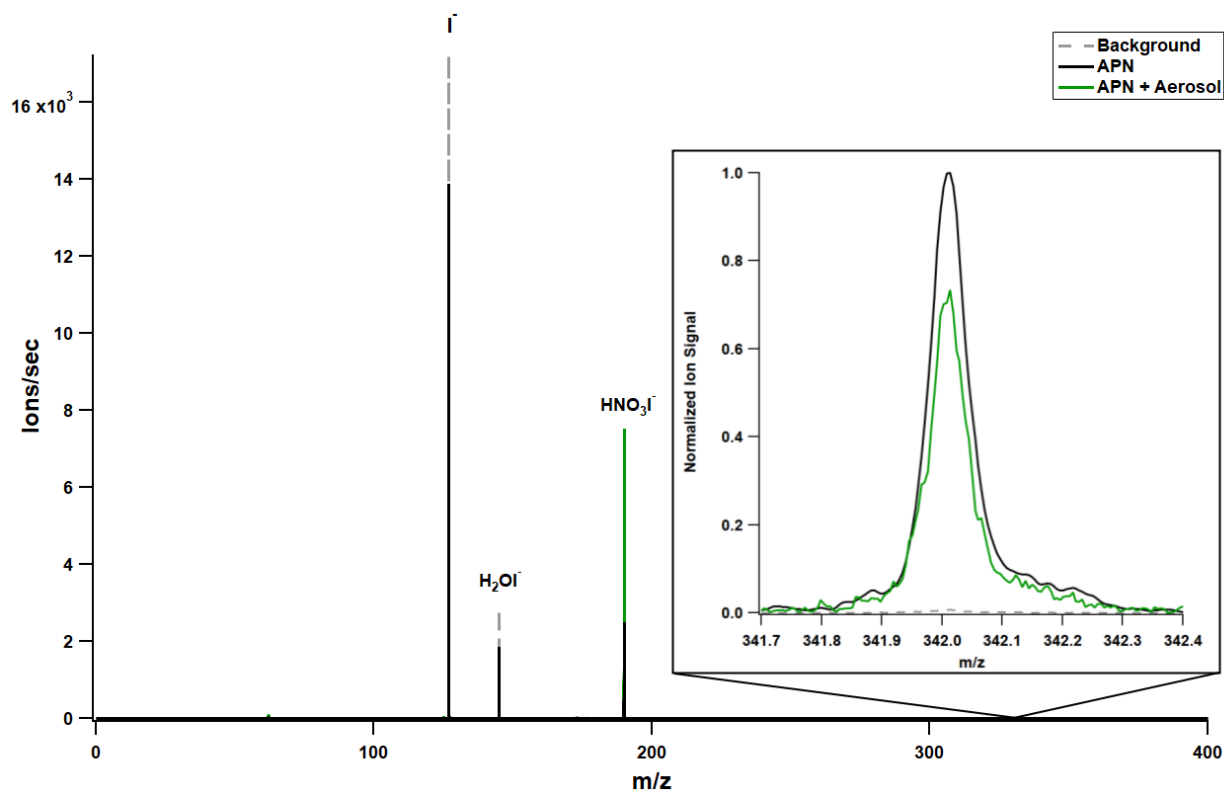
Figure 2.16. Average iodide-adduct CIMS mass spectra of gaseous species for background (dashed gray line), APN injection (black), and APN in the presence of aerosol (green).

Figure 2.17 reveals that the most dominant signal, the reagent ion, I^- ($m/z = 127$),

decreased over the course of all experiments as aerosol was added in the presence of continuous

injection of gaseous APN. As aerosol was added to the system and APN partitioned from the gas

to the particle phase, APN can hydrolyze and form HNO_3 (Perraud et al., 2012). The signal for

HNO_3 ($HNO_3\text{-}I^-$; m/z 189) increased significantly following the addition of ammonium sulfate

seed aerosol in the presence of APN (shown in green shaded area), a clear indication that APN

partitioning and reaction in the aerosol phase occurred on the timescale of the experiment. We

note that the presence of HNO_3 titrates the I^- signal due to its high acidity and affinity for I^-.

While the concentration of I^- added to the ion molecule reactor can affect the total ion abundance

and thus signal intensity of all analytes, there was no clear indication that the resulting depletion

of I^- due to its clustering with HNO_3 affected the APN signal.
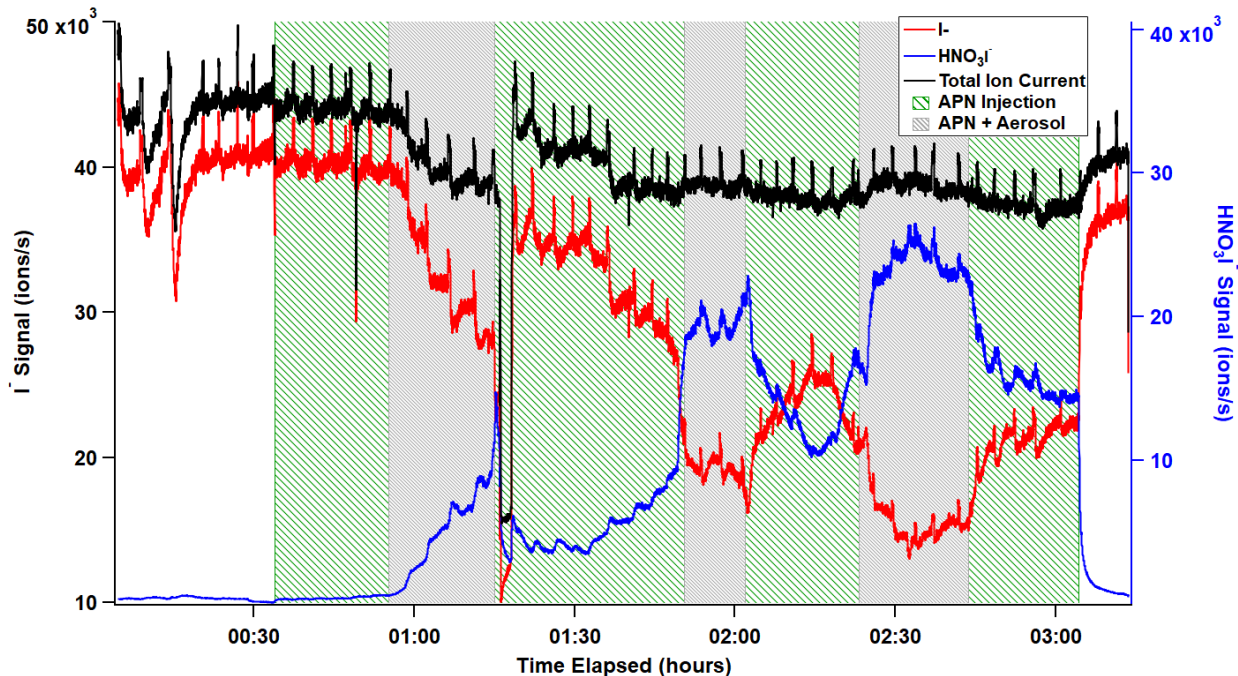
Figure 2.17. Time series of reagent ion, I⁻ (red), HNO₃-I⁻ cluster (blue), and total ion current (black). The shaded regions indicate times when only APN was present (green) and when APN was mixed with aerosol (gray). The systematic "blips" in signal are attributed to constant irregularities in flow originating from the atomizer.

Thus, normalizing to the iodide signal as performed in other similar studies (e.g., Slade et al., 2017; Xiong et al., 2015) would not accurately reflect the losses of APN due to heterogeneous reactions with ammonium sulfate, since normalization to iodide would be weighted heavily by the effects from HNO_3 clustering with I-. Instead, the observed loss rates, uptake coefficients, and mass accommodation coefficients of APN presented in this thesis are determined from the depletion in the raw signal of APN before and after adding the seed aerosol.

2.5 Experimental wall losses in the OFR

APNs are semi-volatile and thus some APN can adsorb to the walls of the chamber, causing additional loss of APN unrelated to uptake onto aerosol. Similarly, hydrolysis products such as HNO_3 are sticky and thus lead to "memory" effects due to adsorption onto the walls.

This is clearly indicated by the accumulation of the HNO_3-I^- cluster (blue) in Fig. 2.17 following

multiple APN injections. Although the wall loss effect is already accounted for since we

established the APN signal in the presence of the wall with aerosol as the only independent

variable, a separate experiment was conducted to elucidate the rate of gas phase APN wall loss in

the PAM-OFR under the conditions of the study. The experiment was conducted at the same

flow rates as in the uptake experiments. The syringe pump equipped with the PAM-OFR injected

50 μL of APN into the chamber with 5 LPM dilution flow to maintain flow rates that were

consistent with those during the uptake experiments. The rate of APN loss by adsorption to the

walls was calculated using Eq. 2.10.

$$k_{loss,obs} = k_{loss,dilution} + k_{loss,wall} \tag{2.10}$$

$k_{loss, obs}$ is the total observed loss of the APN in the absence of aerosol (i.e., only dilution

and loss to the walls), $k_{loss, dilution}$ is the calculated rate of decay due to dilution from continuous

air flow through the PAM-OFR, and $k_{loss, wall}$ is the rate of APN loss to the walls, assuming there

were no other loss processes occurring. $k_{loss,dilution}$ is calculated using the initial signal of APN

and the residence time to calculate the expected rate of decay. Then, the integrated rate law was

used to deduce k, as shown in Eq 2.11.

$$\frac{d[APN]_{loss,dilution}}{dt} = k[APN]_0 \tag{2.11}$$

$k_{loss,obs}$ was calculated by using the first-order rate law described in Eq. 2.7. The difference in

$k_{loss,obs}$ and $k_{loss,dilution}$ is the calculated $k_{loss,wall}$. Figure 2.18 shows the calculated total loss

(squares), loss from dilution (triangles), and wall loss (circles). Note that the total loss is the sum

of dilution and wall loss. While a significant concentration of the APN that entered the PAM-

OFR was depleted prior to exiting the PAM-OFR, most of the APN depletion can be attributed to

dilution, whereas wall losses account for <10% of the total loss with a calculated first-order wall loss rate of 4.85×10^{-5} s^{-1}.
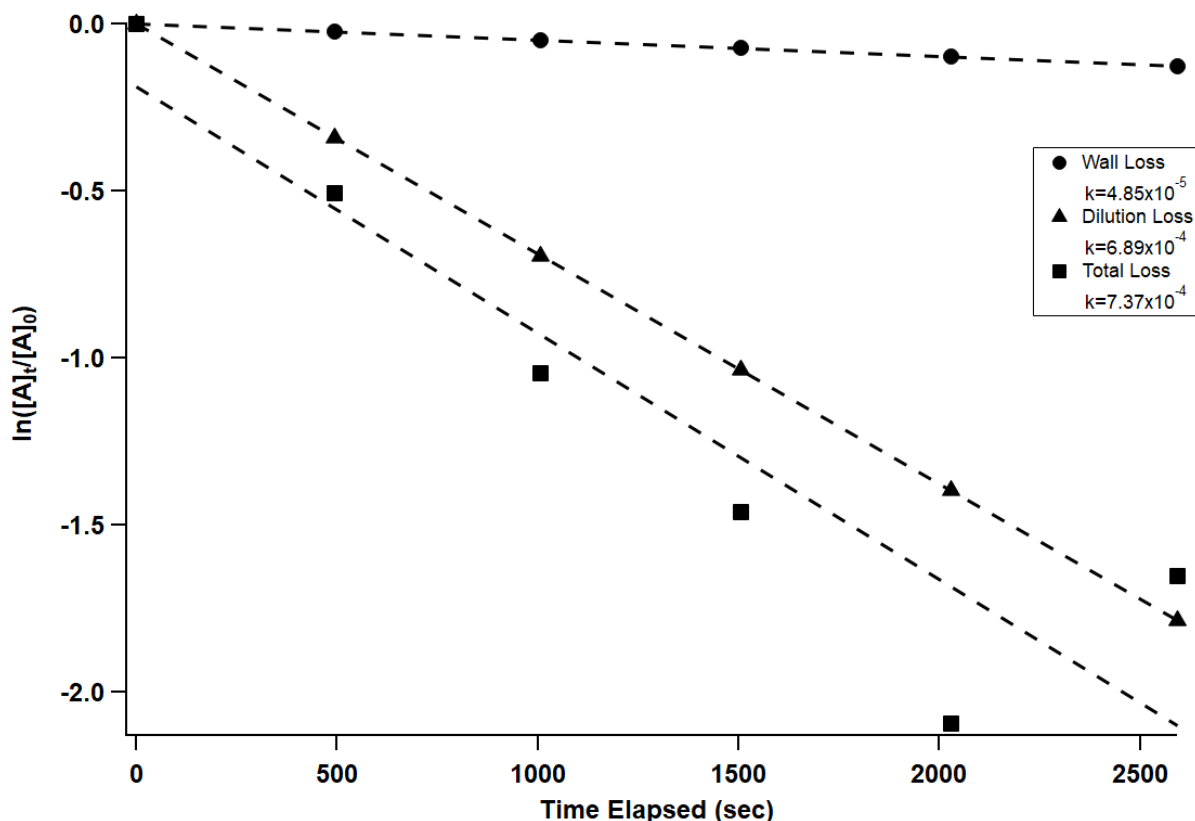
Figure 2.18. Observed first-order rate loss of APN and calculated loss of APN due to dilution flow through the PAM and wall loss.

Changes in RH may also affect the rate of loss of APN to the walls as water molecules adhere to the walls of the PAM-OFR and alter the composition of the surface. Given that the only independent variable in these studies was the concentration of aerosol added to the PAM-OFR and that the APN signal was allowed to establish regardless of the RH in the PAM-OFR, no wall loss or dilution corrections were applied in this study. As discussed previously and shown in Fig. 2.7, we did correct the APN signal depletion due to the increase in RH when aerosol was added to the PAM-OFR in the presence of APN.

CHAPTER 3: RESULTS AND DISCUSSION

3.1 Uptake of APN onto $(NH_4)_2SO_4$ seed aerosol

Figure 3.1 displays the time series for the corrected APN signal from the CIMS over the course of an example uptake experiment. The time series for all other experiments were similar, so only experiment 5 (i.e., neutral seed, low RH) is presented here for visualization. For this experiment, there was a significant enhancement in RH by ~15% following the addition of the seed aerosol particles across the three trials shown. As described previously, changes in RH can affect the sensitivity of iodide-adduct formation with APN. Any observed decrease in APN signal because of increased RH therefore must be accounted for to isolate the loss of APN due to uptake to the seed aerosol only. Here, the changes in RH were calculated by taking the difference of the RH in the PAM-OFR before aerosol introduction and the RH at each time point. This difference corresponds to a percent change of signal, which is applied to the APN signal as a correction, resulting in an ~8% correction. A linear drift correction was also applied, i.e., by linearly interpolating the APN mass spectra signal during uptake based on the drift in the average APN signal before aerosol was added and after aerosol flow was stopped. Signal drift can occur, e.g., because of decay of APN in the purified sample over time, different wall loss coefficients as the seed aerosol adsorbs and sticks to the walls thus altering the equilibrium of APN on the walls and in the gas phase of the PAM-OFR, gradual changes in temperature and RH, and instrument noise.
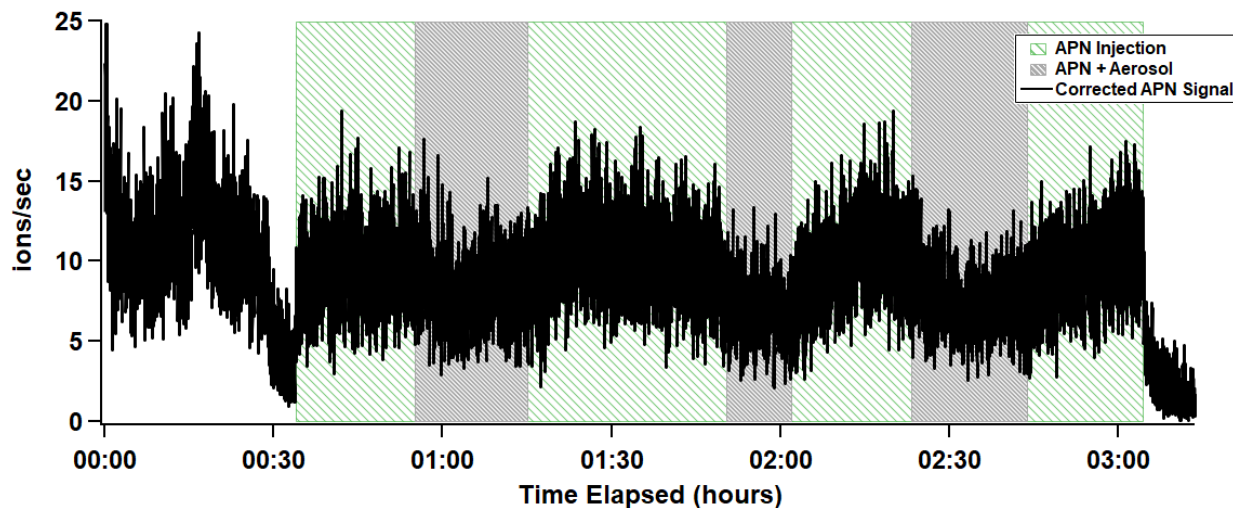
Figure 3.1. Time series of the gas phase APN signal from the CIMS. Beginning of experiment is demarcated with first injection of APN. APN signal is corrected for sensitivity changes from RH changes and signal drift.

After corrections, however, there was still an observed loss of APN in the presence of seed aerosol and a restoration of the APN signal after aerosol flow was stopped, indicative of loss of APN due to reactive uptake. Additional evidence of APN uptake into the aerosol can be seen in the time series of NO_2^- and NO_3^- in the particle phase, shown in Figure 3.2. This time series was from an experiment performed under the same environmental conditions as experiment 5, except EESI-TOF was used to measure aerosol-phase species. In the experiments using EESI-TOF, seed aerosol was introduced to the PAM-OFR first followed by injection of APN in the gas phase. Figure 3.6 shows that NO_3^- and NO_2^- signals increased after APN injection, indicative of APN uptake onto the seed aerosol and subsequent hydrolysis to form HNO_3. The NO_3^- signal measured in the particle-phase with EESI-TOF can be attributed to the following reaction equilibria:

$$HNO_3 + H_2O \leftrightarrow H_3O^+ + NO_3^- \hspace{3cm} 3.1$$

39
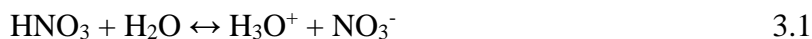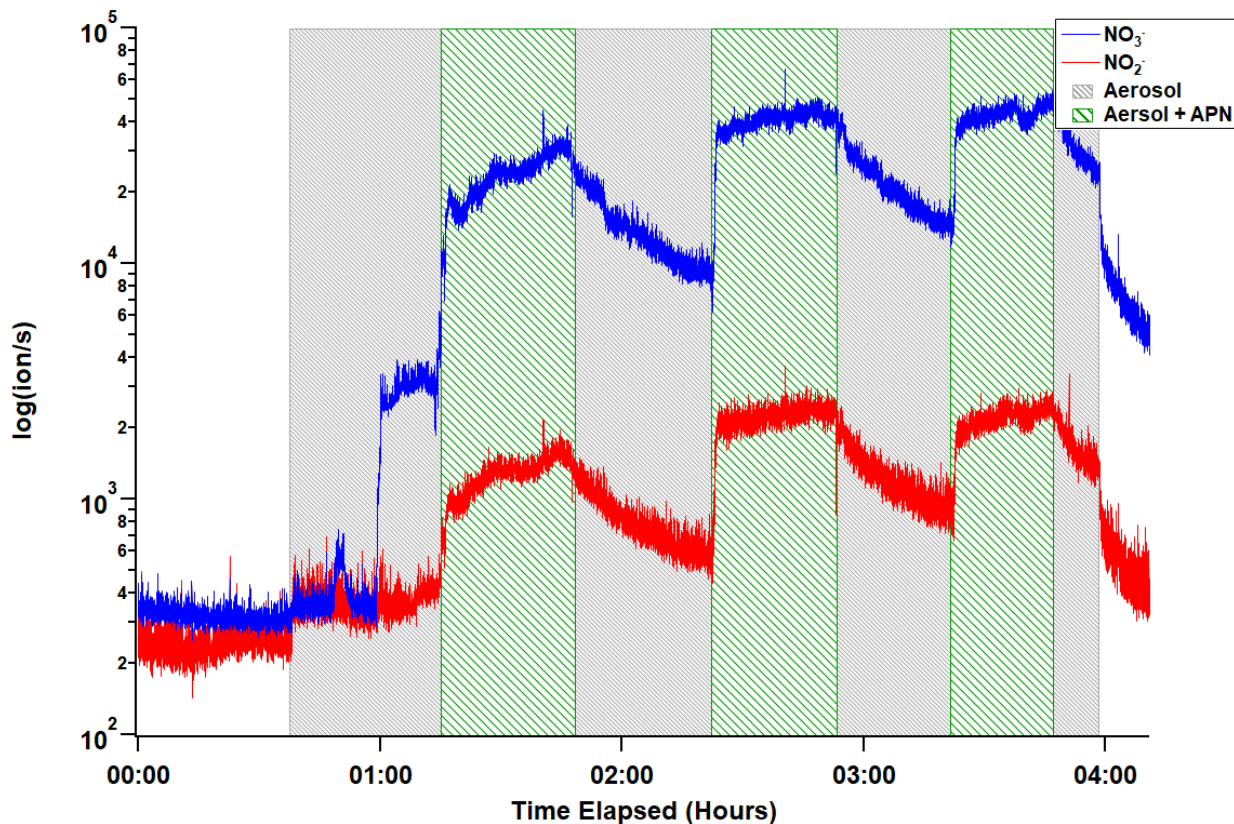
Figure 3.2. Time Series of NO_2^- and NO_3^- from Experiment 5 Using EESI TOF-MS.

3.3.1 Observed APN loss rate (pseudo first-order kinetics)

Pseudo-first order uptake kinetics of APN uptake by ammonium sulfate seed aerosol were calculated from the observed reduction in the APN signal in the gas phase after introducing aerosol following Eq. 2.7. The natural logarithm of the ratio of the APN signal over time, t (~166 s), the residence time in the OFR, and APN signal before aerosol injection (t_0=0 s) was plotted as a function of the residence time and the resulting slope represents the pseudo-first order loss rate, k_1. The average decay curves for APN under the different experimental conditions studied here are shown in Fig. 3.3. From k_1, we calculated mass accommodation coefficients (α) and reactive uptake coefficients (γ), the results of which are shown for the different experimental conditions in Table 3.1 and will be described in the following sections.

40

Table 3.1. Average observed loss rates (k), reactive uptake coefficients (γ), and mass accommodation coefficients (α) at different RH for acidic seed and "neutral" seed aerosol experiments.

	Particle Acidity	RH	k (s^{-1})	γ	α
1	Acidic Seed	90%	1.63E-03±3.99E-04	2.26E-04±5.54E-05	4.00E-04±9.79E-05
2	Acidic Seed	70%	1.16E-03±2.94E-04	7.25E-04±1.95E-04	2.29E-03±4.43E-04
3	Neutral Seed	90%	1.14E-03±8.49E-04	1.07E-04±7.98E-05	1.98E-04±1.48E-04
4	Neutral Seed	70%	8.84E-04±1.28E-04	8.60E-05±1.20E-05	1.54E-04±2.23E-05
5	Neutral Seed	25%	7.58E-04±1.77E-04	1.27E-04±2.97E-05	3.31E-04±7.84E-05
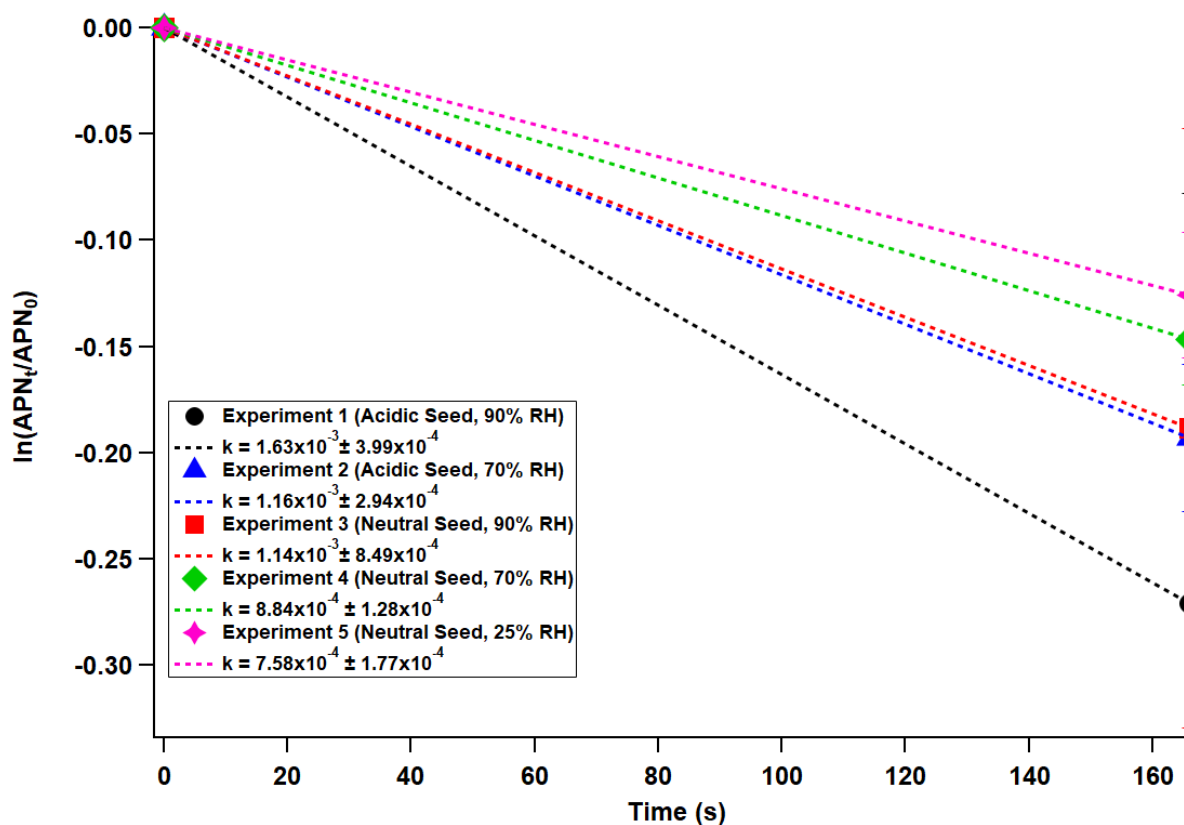
Figure 3.3. Pseudo-first order decay of APN at different RH and seed particle acidity.
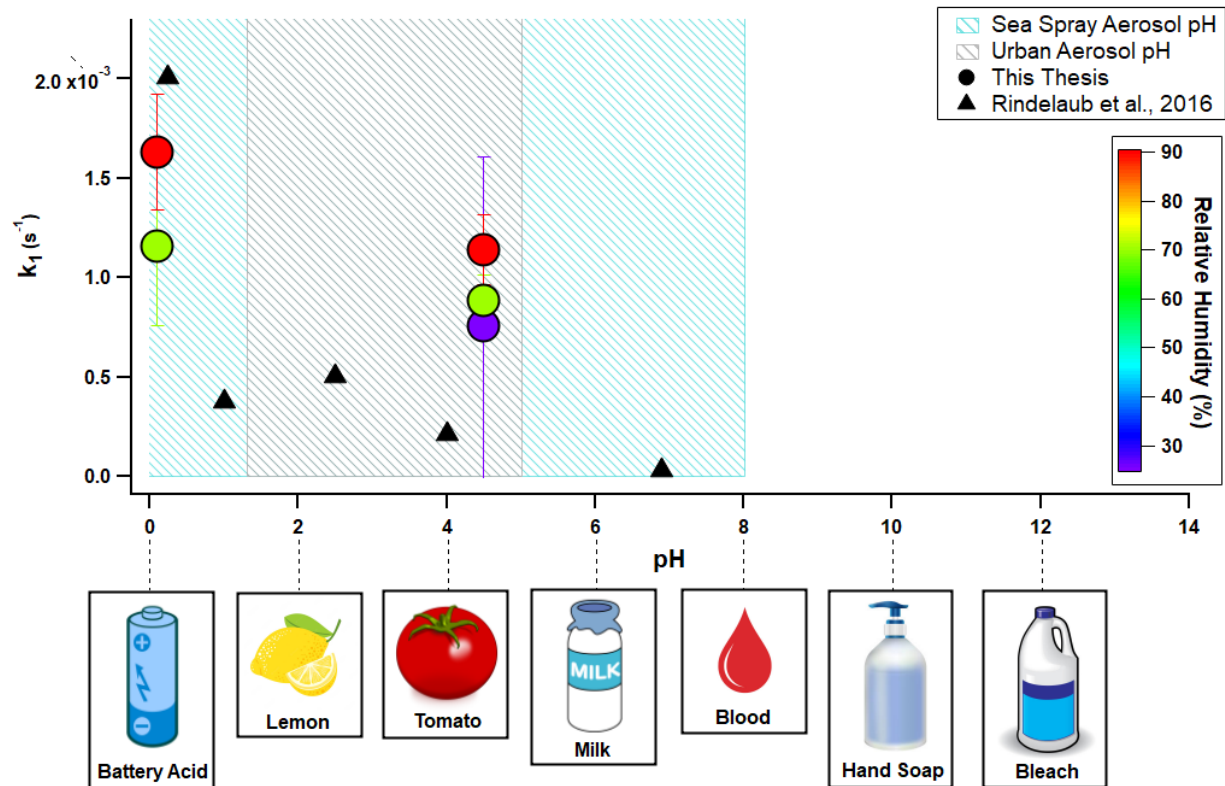
Figure 3.4. Observed loss rates of APN by ammonium sulfate seed aerosol from this work (circles) and hydrolysis rates from Rindelaub et al., 2016 (triangles) at different RH and aerosol pH. The shaded regions represent different aerosol pH ranges for urban aerosol (gray) (Zhang et al., 2021; Battaglia jr. et al., 2021; Arangio et al., 2022) and sea spray aerosol (Winkler et al., 1986; Fridlind et al., 2000; Keene et al., 2002; Pszenny et al., 2004; Kroll et al., 2015; Bougiatioti et al., 2016; Dall'Osto et al., 2019; Angle et al., 2020). The error bars assigned here are from the calculated standard deviations in the observed loss rates between separate trials.

Observations of gas phase APN loss reveal that the observed loss rates increase with both increasing seed particle acidity and RH. Under acidic conditions, k_1 increased relative to the neutral-seed aerosol at RH=70% and RH=90% by 32% and 43%, respectively. k_1 also increased with increasing RH for APN uptake by the "neutral" seed aerosol. Increasing RH from 25% to 70% led to an enhancement in k_1 of 14% while increasing RH from 70% to 90% led to an enhancement in k_1 of 29%.

The increasing observed loss rate with decreasing aerosol pH is likely attributed to the acid-catalyzed hydrolysis of APN. Hydrolysis of organic nitrates is hypothesized as the dominant

pathway for organic nitrate loss in the atmosphere (Day et al., 2011; Russell et al., 2011), which may be acid-catalyzed (Allen et al., 1953). The acid in the system acts as a proton donor to the nitrate group and the formed nitric acid becomes a leaving group, forming a tertiary carbocation (Figure 3.5). The increased acidity of the particles would lead to more free protons in the system to initiate the hydrolysis process, explaining the significant increase in the observed loss rate with increasing acidity. Increasing RH also led to an enhanced loss of APN, as in the case of APN uptake onto neutral seed ammonium sulfate at RH=25% compared to RH=70% and RH=90%, which may be driven by hydrolysis in the absence of added acid. Water is a reactant in this reaction; thus, it is expected that excess reactant at the higher RH would increase the rate of reactive loss of APN by hydrolysis. Ammonium sulfate is hygroscopic and following atomization is expected to remain in a deliquesced-like (liquid) physical state when RH=70% and RH=90%. Hygroscopic mass growth (i.e., ratio of wet particle diameter-to-dry diameter) of ammonium sulfate aerosol following dehydration from fully deliquesced (i.e., RH>80%) to RH=70% is a factor of two larger in diameter than dried ammonium sulfate. Increasing RH to 90% leads to a wet particle size that is ~3.5x the diameter of dried ammonium sulfate (Vlasenko et al., 2017). When dried to RH=25%, ammonium sulfate undergoes efflorescence (i.e., crystallization). As such, under these conditions, less liquid water in the aerosol matrix is available to react with APN following its adsorption to the particle surface. In contrast, at a relatively high RH (70% or 90%) enough aerosol liquid water is available to hydrolyze APN. In addition, APN can diffuse more readily from the particle surface to the bulk due to the plasticizing effects of water and hence react (i.e., hydrolyze) to a greater extent with water available in the particle bulk.
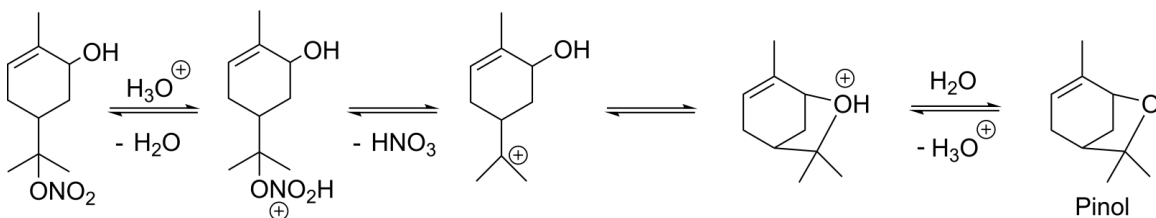
Figure 3.5. The Theorized Acid-Catalyzed Hydrolysis of Alpha Pinene Hydroxynitrate (Rindelaub et al., 2016)

Increasing particle acidity and RH accelerated the observed loss rate. However, k_1 is apparently much more sensitive to changes in pH in comparison to changes in RH. For example, k_1 for APN uptake onto neutral seed ammonium sulfate aerosol increased by 14% when increasing RH from RH=70% to RH=90%, whereas k_1 increased by 29% from RH=70% to RH=90% when the ammonium sulfate seed aerosol was acidified with H_2SO_4. These experiments reveal that APN uptake rates are driven by pH rather than RH, which is consistent with findings from other experiments investigating the hydrolysis rates of other tertiary organic nitrates (Rindelaub et al., 2015; Rindelaub et al., 2016; Morales et al., 2021). Previous studies have shown that hydrolysis rates of organic nitrates increase with increasing alkyl substitution as well (Bean and Hildebrandt Ruiz 2016; Boyd et al., 2015, 2017; Darer et al., 2011; Hu et al., 2011; Liu et al., 2012; Ng et al., 2017), which is theorized to derive from the allylically stabilized tertiary carbocation that is formed after nitrate is abstracted. Based on the observed decay of APN signal in the CIMS, the observed loss rates of APN onto seed aerosol were calculated to be $9.22 \times 10^{-4} - 1.86 \times 10^{-3}$ s^{-1}, which is on the same order of magnitude (but less) than the hydrolysis rates of the same APN isomer studied previously in bulk aqueous solutions (Rindelaub et al., 2015; Rindelaub et al., 2016). The greater hydrolysis rates in Rindelaub et al., 2016 are likely due to the hydrolysis experiments being performed in the bulk aqueous phase in comparison to

44

the uptake onto aerosol in the chamber experiments performed here. There are different kinetic limitations to consider for heterogeneous reactions: (1) APN must first adsorb and "stick" to the particle surface. The efficiency at which the gas molecules stick to the aerosol surface is determined by the mass accommodation coefficient and depends on the type of aerosol surface on which APN adsorbs and the reactivity between APN and the particle. (2) Depending on its reactivity, APN may be mobile and diffuse on the particle surface prior to absorbing and reacting in the bulk instead of already being incorporated in the bulk as in other studies. The rate of diffusion into the particle bulk can depend on the viscosity of the particle (Perraud et al., 2012). For more solid-like aerosol, as in the case of effloresced ammonium sulfate seed aerosol, molecular diffusion can be limited and thus (3) reactions are limited more to the surface than in the bulk in our experiments compared to other studies. Upon particle deliquescence, APN can diffuse and may react more readily in the particle bulk. This is perhaps why our measured first-order heterogeneous loss rates at RH=90% are in better comparison with the hydrolysis rate constants for APN reported in bulk water in Rindelaub et al., 2016, which were measured as 2.14×10^{-4} under neutral conditions and 2.01×10^{-3} under acidic conditions. The differences between our measured loss rates and previously reported hydrolysis rates are minor, which implies that hydrolysis is likely the major pathway for heterogeneous loss of APN onto ammonium sulfate seed aerosol.

3.3.2 Reactive uptake coefficient

From the observed first-order loss rate, we can isolate the loss of APN due to reaction upon collision with the surface by calculating the reactive uptake coefficient (γ), defined as the ratio of total molecules removed from the gas phase relative to the total number of gas-particle

collisions (Liggio et al., 2005). γ was calculated using Eq. 2.8. Here, the surface area

concentration term (S_a) was derived from the measured aerosol surface area concentration of

unreacted ammonium sulfate, i.e., prior to introducing APN to the chamber in the gas phase.
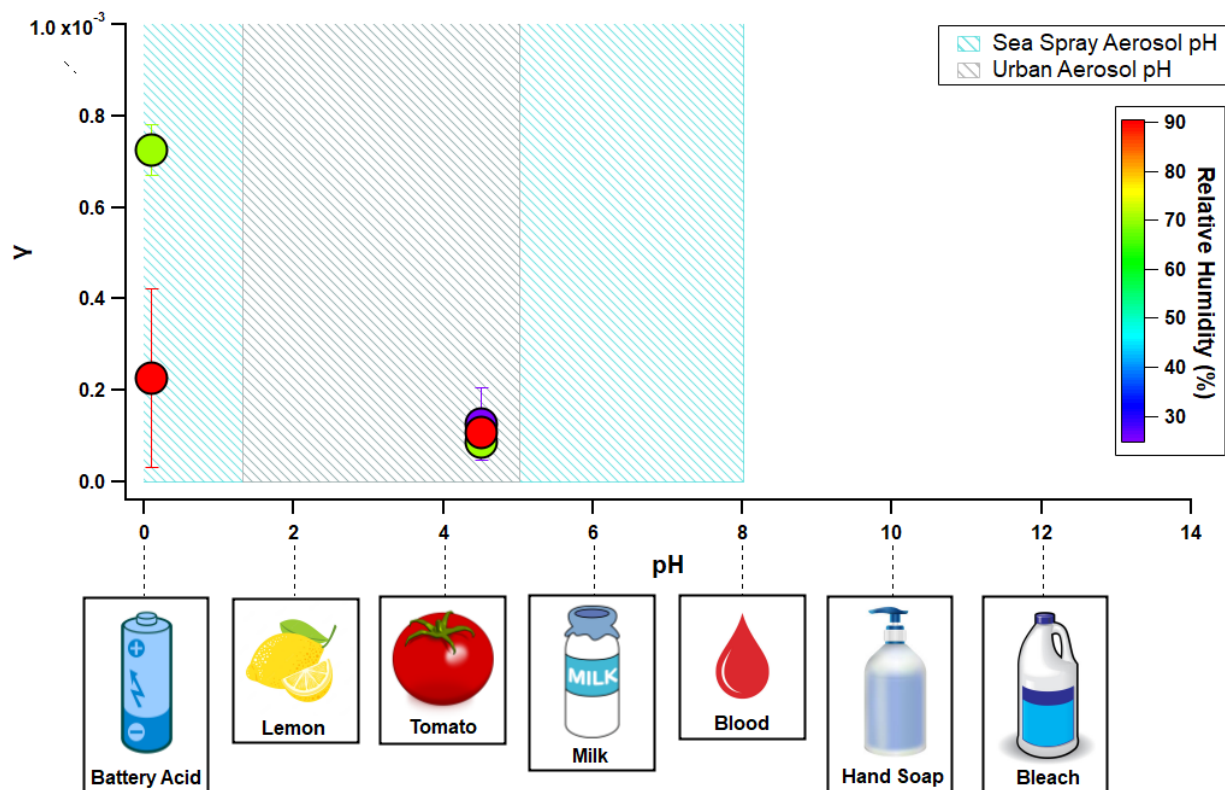
Figure 3.6. Calculated Reactive Uptake Coefficients at Different Seed Particle Acidities and RH values. The error bars assigned here are from the calculated standard deviations between separate trials.

Figure 3.6 and Table 3.1 show γ for APN uptake by ammonium sulfate seed aerosol

under the different experimental conditions studied. γ increased with increasing seed particle

acidity as did k_1, whereas it decreased with increasing RH, in contrast to k_1. The similar

dependence on pH demonstrates that the first-order loss rate of APN is dictated by the

heterogeneous reactivity between APN and the aerosol. In analogy to the discussion in Sec.

3.3.1, the heterogeneous uptake kinetics here could be driven by an acid-catalyzed hydrolysis

mechanism, as has been observed previously for similar acid-catalyzed chemistry involving

isoprene-derived epoxydiols in aerosol (Gaston et al., 2014; Nguyen et al., 2014). To date, only one other study has experimentally determined γ of organic nitrates following uptake onto aerosol (Vander Wall et al., 2018). In that study, γ was measured for three different commercially-available organic nitrates in the presence of model organic aerosol particles and showed γ values ranged from $\sim10^{-5}$ for ethyl hexyl nitrate to $\sim10^{-3}$ for a corresponding hydroxy nitrate, in a similar range as γ in this study. This thesis also observed trends in γ with changing RH that are consistent with Gaston et al., 2014 and Nguyen et al., 2014, in which γ decreases with increasing RH. In their study, the increase in γ with decreasing RH was attributed to a so-called "burying" mechanism whereby unreacted organic nitrates that adsorbed and remained mobile on the organic aerosol surface became "buried" in the particle phase due to the condensation of other oxidized organic species present. While a direct comparison between this work and the study by Vander Wall et al., 2018 cannot be made due to differences between experimental conditions, organic nitrate precursor, and seed particle/substrate, their results highlight that the measured γ for APN uptake by dry ammonium sulfate seed aerosol (i.e., least reactive aerosol system) could be driven by such a burying process rather than hydrolysis. This burying mechanism could also be important in the relatively high RH, acidic seed experiments, whereby unreacted APN becomes buried in the particle phase by formation of lower-volatility hydrolysis products, which include alpha-pinene diols and acid-catalyzed oligomers (Surratt et al., 2010). In a different comparison, Gaston et al., 2014 found that the γ value for an isoprene-derived epoxydiol (IEPOX) onto seed particles with a similar acidity to our experiments was 2×10^{-4}. This value is slightly less (indicating slower reactivity) than what was experimentally determined here (2.24×10^{-4}). The greater reactivity could be due to the nitrate group on APN,

which acts as a better leaving group than the diols, leading to faster reactive uptake and thus a larger uptake coefficient.

3.3.2 Mass accommodation coefficient

To better understand the gas uptake process of APN by ammonium sulfate seed aerosol, the mass accommodation coefficients (α), also known as the sticking probability, were calculated at different RH and pH. α is the probability that a gas molecule, upon collision with the aerosol phase, gets incorporated in the aerosol, and is affected by the rate of adsorption and reaction between the gas and components in the particle phase. While α is affected by heterogeneous reactivity, it is important to note that it is not equivalent to γ. The difference in α and γ, in fact, represents the fraction of gas molecules that get incorporated in the aerosol but do not react.
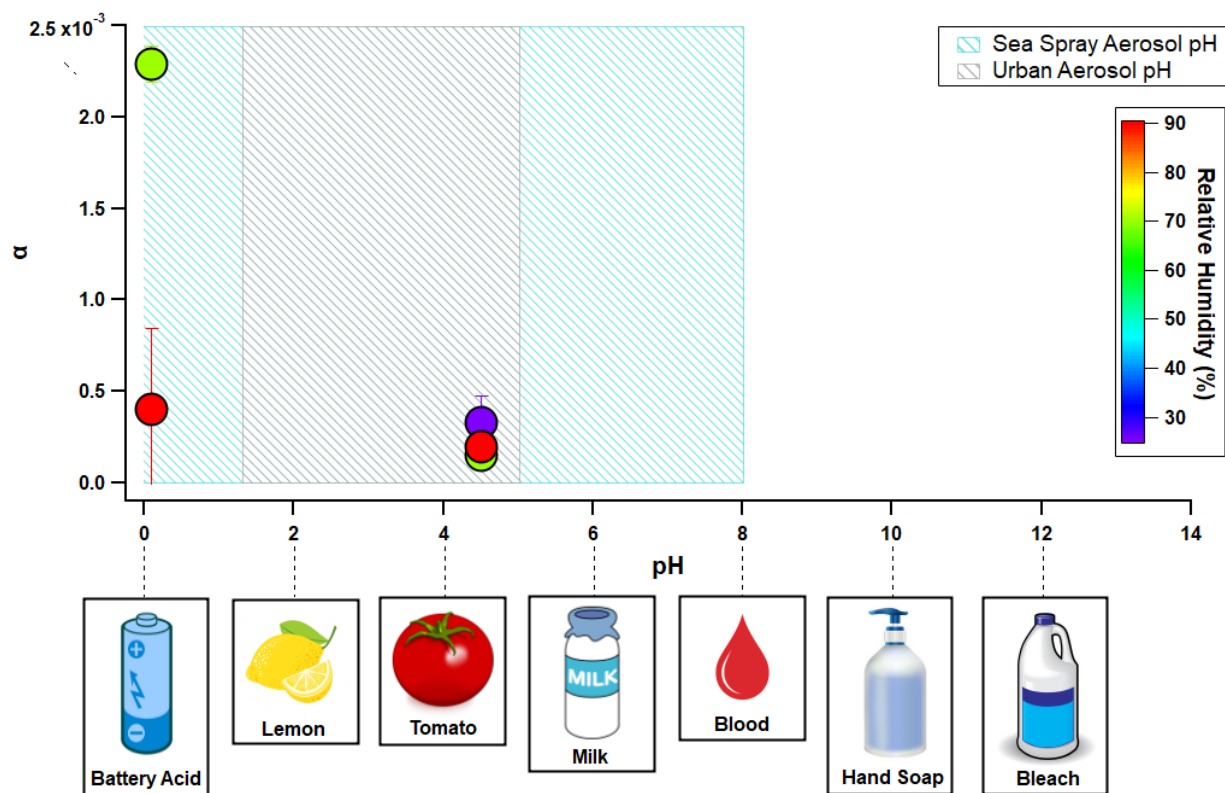
Figure 3.7. Calculated mass accommodation coefficients at different seed particle acidities and RH values. The error bars assigned here are from the calculated standard deviations between separate trials.

48

α was calculated using the Fuchs-Sutugin approach (Fuchs and Sutugin, 1970) using Eq. 2.9. Figure 3.7 and Table 3.1 show how α differed under the different experimental conditions in this study. The measured α values indicate a relatively low probability of APN sticking to the aerosol surface upon collision. Previous studies show α for other organic nitrates range from 1 to 0.001 (Liu et al., 2019; Pound, 1972; Saleh et al., 2013; Grieshop et al., 2007; Grieshop et al., 2009; Zhang et al., 2014), meaning that only in the presence of acidic seed aerosol at RH=70% is APN mass accommodation within previously observed ranges. Previous studies have found that the volatility of the gas phase organic nitrate drives mass accommodation (Krechmer et al., 2017). Using a model to calculate α for APN based on its pure compound volatility (Capouet et al., 2006; Liu et al., 2019, Shiraiwa and Pöschl 2021), α was predicted to be an order of magnitude larger than what was measured. This implies that for the APN system, α was affected by factors other than volatility. These factors could include but are not limited to aerosol phase, other gas phase constituents that adsorb first or co-adsorb with APN, and mass accommodation time scales.

The gas phase constituents studied in previous experiments are lower volatility than APN. As the molecules in the aerosol repartition and reach equilibrium with their gas-phase concentrations (Grieshop et al., 2007), more of these lower volatility gases will remain in the particle phase compared to APN. Although more studies are needed to elucidate the mechanisms that impact α for APN, the α values presented in this thesis increased with seed particle acidity, which is consistent with γ and k_1 calculated in this work and in previously described studies (Darer et al., 2011; Hu et al., 2011; Liu et al., 2012; Nguyen et al., 2014; Gaston et al., 2014; Boyd et al., 2015; Boyd et al., 2015; Rindelaub et al., 2015; Rindelaub et al., 2016; Bean and Hildebrandt Ruiz 2016; Boyd et al., 2017; Ng et al., 2017; Morales et al., 2019; Takeuchi and

Ng 2019). Trends in α with pH and RH were consistent with γ and were observed to increase with decreasing RH. The acidic seed case at RH=70% had the highest α, suggesting that the liquid states and acidity of the seed aerosol promote transfer of APN from the gas to the particle phase. Under more acidic conditions, APN will form a larger quantity of lower volatility, acid-catalyzed oligomerization products (Perraud et al., 2012). At higher RH, these products may form more rapidly potentially increasing the viscosity of the aerosol and hinder the mass transfer of unreacted APN to the particle phase, leading to the decrease in α as RH increased. As the structure and composition of aerosol becomes more complex, heterogenous interactions with APN become harder to predict and model (Pfrang, Shiraiwa, and Pöschl. 2011), making it important to understand the factors that affect mass accommodation and the way that APN uptake changes particle phase and composition.

CHAPTER 4: CONCLUSIONS, ATMOSPHERIC IMPLICATIONS AND FUTURE WORK

4.1 Conclusions

Heterogeneous reactive uptake coefficients were measured for the first time for an alpha-pinene-derived hydroxy nitrate (APN) following uptake to ammonium sulfate aerosol at different RH and particle acidity. First-order loss rates were on the order of 1.6×10^{-3} s^{-1} – 7.6×10^{-4} s^{-1}, which increased with increasing particle acidity and RH. We attribute the enhanced first-order loss rates by uptake onto acidified seed particles to acid-catalyzed hydrolysis of APN, which has been theorized to be the main aerosol sink of organic nitrates. Increased RH led to increased observed loss rates of APN due to the additional reactant, H_2O, which participated in the hydrolysis of APN. However, the observed loss rates of APN due to increasing RH were less pronounced than with increasing seed particle acidity. Additional liquid water in the particle phase at high RH is hypothesized to reduce the nucleophilic strength of the bulk aerosol solution, which slows down the initiation of the hydrolysis mechanism. This attenuation in the observed loss of APN, however, is not enough to completely overcome the additional ionic strength due to the presence of the acid in acidic seed particles.

Reactive uptake coefficients were measured to be 1.0×10^{-4} – 7.3×10^{-4}. Like the observed first-order loss of APN, γ increased with increasing seed particle acidity. However, after accounting for changes in particle surface area due to the growth of the particles at higher RH, the fraction of reactive collisions between APN and ammonium sulfate aerosol decreased with increasing RH, in contrast to k_1. The enhanced reactive uptake coefficients with increasing seed particle acidity implies that the acid-catalyzed hydrolysis is a significant driver in the heterogeneous reactive uptake of APN. The slower reactive uptake of APN measured at the higher RH could result from the reduction in the nucleophilic strength of the aerosol in the

51

presence of a greater fraction of liquid water in the particles. Alternatively, at the lower RH, a potential "burying" mechanism could occur whereby APN gets taken up but does not re-partition to the gas phase due to the formation of a viscous organic layer, in analogy to the study by Vander Wall et al., 2018. Based on the ratio of γ to α, the results suggest that approximately 30-55% of the APN molecules that were accommodated underwent reaction, i.e., 45%-70% of the APN molecules remained mobile (unreacted) after they adsorbed to the particles. This has important implications for the lifetimes of APN after it is taken up by aerosol, which could affect our understanding of secondary organic aerosol growth.

4.2 Atmospheric Implications

The observed first-order loss rates imply a short lifetime of APN in the gas phase in the presence of aerosol under atmospherically relevant conditions. The greater heterogeneous loss of APN with increasing seed particle acidity may be relevant for areas with higher levels of coal burning and industrial manufacturing where reactions between SO_2 and water can lead to the formation of more acidic aerosol. The conversion of semi-volatile APN to lower volatility hydrolysis products in the presence of acidic particles could lead to greater aerosol mass growth, affecting the size of particles and thus atmospheric visibility and the hygroscopicity of aerosol in these areas. The formation of these lower-volatility products could further impact particle physicochemical properties, including phase state (Slade et al., 2019). The formation of APN in the atmosphere acts as a reservoir for NO_x, a precursor to tropospheric ozone. Hydrolysis in the particle phase and the loss of $RONO_2$ may slow the formation of tropospheric ozone. The rates of uptake of APN imply that APN hydrolyzes and removes NO_x from the atmosphere on timescales in which it will not be transported to otherwise "clean air" areas that are downwind from regions with high levels of traffic. These results suggest that the formation and uptake of APN acts as an

effective sink for NO_x and thus slows the production and limits the long-range transport of O_3. The changing uptake rates with different particle pH and RH also emphasizes the need for more ambient measurements of aerosol pH and levels of particulate organic nitrogen under differing environmental conditions.

4.3 Future Work

Further studies could be performed across a wider range of RH and aerosol pH and in the presence of different seed aerosol. More knowledge on the way different atmospheric conditions affect uptake rates can be used for more accurate modeling of urban pollution transport and parametrizations of the fate of NO_x in different regions.

Future work should investigate specifically how uptake of APN affects particle physicochemical properties including phase state, morphology, and hygroscopicity and vice versa. The growth of organic mass on inorganic salt particles is known to alter aerosol interactions with water vapor (Wu et al., 2018). Incorporation of liquid water in the particles can alter particle phase (viscosity) and may promote greater transfer of APN from the particle surface to the bulk in addition to greater hydrolysis rates. Future efforts should evaluate the importance of particle viscosity in modulating the uptake of APN in comparison to hydrolysis. For example, experiments could be performed whereby model hydrophobic aerosols with different viscosities could be introduced in the presence of APN.

This study only considered the heterogeneous reactivity of one isomer of APN, yet we understand from other studies that carbon chain length, location of the nitrate on the molecule (primary, secondary, and tertiary) all impact the hydrolysis rates of organic nitrates. Additional

experiments building off this thesis should consider different isomers of APN to understand how

molecular structure changes the rate of uptake of these important organic nitrates.

REFERENCES

(1)

Aljawhary, D.; Lee, A. K. Y.; Abbatt, J. P. D. High-Resolution Chemical Ionization Mass Spectrometry (ToF-CIMS): Application to Study SOA Composition and Processing. *Atmospheric Measurement Techniques* **2013**, *6* (11), 3211–3224. https://doi.org/10.5194/amt-6-3211-2013.

(2)

Allen, A. D. Hydrolysis of Organic Nitrites. *Nature* **1953**, *172* (4372), 301–302. https://doi.org/10.1038/172301b0.

(3)

Alves, L.; Holz, L. I. V.; Fernandes, C.; Ribeirinha, P.; Mendes, D.; Fagg, D. P.; Mendes, A. A Comprehensive Review of NOx and N2O Mitigation from Industrial Streams. *Renewable and Sustainable Energy Reviews* **2022**, *155*, 111916. https://doi.org/10.1016/j.rser.2021.111916.

(4)

Angle, K. J.; Crocker, D. R.; Simpson, R. M. C.; Mayer, K. J.; Garofalo, L. A.; Moore, A. N.; Mora Garcia, S. L.; Or, V. W.; Srinivasan, S.; Farhan, M.; Sauer, J. S.; Lee, C.; Pothier, M. A.; Farmer, D. K.; Martz, T. R.; Bertram, T. H.; Cappa, C. D.; Prather, K. A.; Grassian, V. H. Acidity across the Interface from the Ocean Surface to Sea Spray Aerosol. *Proceedings of the National Academy of Sciences* **2021**, *118* (2), e2018397118. https://doi.org/10.1073/pnas.2018397118.

(5)

Arangio, A.; Violaki, K.; Rivera, J.-C. Q.; He, M.; Motos, G.; Bragazza, L.; Grossiord, C.; Buttler, A.; Nenes, A. *Atmospheric Acidity and Its Impacts on Macronutrient Deposition and Plant Growth*; EGU22-7977; Copernicus Meetings, 2022. https://doi.org/10.5194/egusphere-egu22-7977.

(6)

Ayres, B. R.; Allen, H. M.; Draper, D. C.; Brown, S. S.; Wild, R. J.; Jimenez, J. L.; Day, D. A.; Campuzano-Jost, P.; Hu, W.; de Gouw, J.; Koss, A.; Cohen, R. C.; Duffey, K. C.; Romer, P.; Baumann, K.; Edgerton, E.; Takahama, S.; Thornton, J. A.; Lee, B. H.; Lopez-Hilfiker, F. D.; Mohr, C.; Goldstein, A. H.; Olson, K.; Fry, J. L. *Organic Nitrate Aerosol Formation via NO₃ + BVOC in the Southeastern US*; preprint; Aerosols/Field Measurements/Troposphere/Chemistry (chemical composition and reactions), 2015. https://doi.org/10.5194/acpd-15-16235-2015.

(7)

Baker, J. W.; Easty, D. M. Hydrolysis of Organic Nitrates. *Nature* **1950**, *166* (4212), 156–156. https://doi.org/10.1038/166156a0.

(8)

Battaglia Jr., M. A.; Balasus, N.; Ball, K.; Caicedo, V.; Delgado, R.; Carlton, A. G.; Hennigan, C. J. Urban Aerosol Chemistry at a Land–Water Transition Site during Summer – Part 2: Aerosol PH and Liquid Water Content. *Atmospheric Chemistry and Physics* **2021**, *21* (24), 18271–18281. https://doi.org/10.5194/acp-21-18271-2021.

(9)

Bean, J. K.; Hildebrandt Ruiz, L. Gas–Particle Partitioning and Hydrolysis of Organic Nitrates Formed from the Oxidation of <I>A</I>-Pinene in Environmental Chamber Experiments. *Atmos. Chem. Phys.* **2016**, *16* (4), 2175–2184. https://doi.org/10.5194/acp-16-2175-2016.

(10)

Bell, M. L.; Kim, J. Y.; Dominici, F. Potential Confounding of Particulate Matter on the Short-Term Association between Ozone and Mortality in Multisite Time-Series Studies. *Environmental Health Perspectives* **2007**, *115* (11), 1591–1595. https://doi.org/10.1289/ehp.10108.

(11)

Bell, M. L.; McDermott, A.; Zeger, S. L.; Samet, J. M.; Dominici, F. Ozone and Short-Term Mortality in 95 US Urban Communities, 1987-2000. *JAMA* **2004**, *292* (19), 2372–2378. https://doi.org/10.1001/jama.292.19.2372.

(12)

Bertram, A. K.; Martin, S. T.; Hanna, S. J.; Smith, M. L.; Bodsworth, A.; Chen, Q.; Kuwata, M.; Liu, A.; You, Y.; Zorn, S. R. Predicting the Relative Humidities of Liquid-Liquid Phase Separation, Efflorescence, and Deliquescence of Mixed Particles of Ammonium Sulfate, Organic Material, and Water Using the Organic-to-Sulfate Mass Ratio of the Particle and the Oxygen-to-Carbon Elemental Ratio of the Organic Component. *Atmospheric Chemistry and Physics* **2011**, *11* (21), 10995–11006. https://doi.org/10.5194/acp-11-10995-2011.

(13)

Bharti, S.; Roy, R. Quantitative 1H NMR Spectroscopy. *TrAC Trends in Analytical Chemistry* **2012**, *35*, 5–26. https://doi.org/10.1016/j.trac.2012.02.007.

(14)

Boschan, R.; Merrow, R. T. The Chemistry of Nitrate Esters. 26.

(15)

Bougiatioti, A.; Nikolaou, P.; Stavroulas, I.; Kouvarakis, G.; Weber, R.; Nenes, A.; Kanakidou, M.; Mihalopoulos, N. Particle Water and PH in the Eastern Mediterranean: Source Variability and Implications for Nutrient Availability. *Atmospheric Chemistry and Physics* **2016**, *16* (7), 4579–4591. https://doi.org/10.5194/acp-16-4579-2016.

(16)

Boyd, C. M.; Sanchez, J.; Xu, L.; Eugene, A. J.; Nah, T.; Tuet, W. Y.; Guzman, M. I.; Ng, N. L. Secondary Organic Aerosol Formation from the β-Pinene+NO$_3$ System: Effect of Humidity and Peroxy Radical Fate. *Atmos. Chem. Phys.* **2015**, *15* (13), 7497–7522. https://doi.org/10.5194/acp-15-7497-2015.

(17)

Boyd, C. M.; Nah, T.; Xu, L.; Berkemeier, T.; Ng, N. L. Secondary Organic Aerosol (SOA) from Nitrate Radical Oxidation of Monoterpenes: Effects of Temperature, Dilution, and Humidity on Aerosol Formation, Mixing, and Evaporation. *Environ. Sci. Technol.* **2017**, *51* (14), 7831–7841. https://doi.org/10.1021/acs.est.7b01460.

(18)

Brown, S. S.; Stutz, J. Nighttime Radical Observations and Chemistry. *Chem. Soc. Rev.* **2012**, *41* (19), 6405. https://doi.org/10.1039/c2cs35181a.

(19)

Browne, E. C.; Cohen, R. C. Effects of Biogenic Nitrate Chemistry on the NO$_x$ Lifetime in Remote Continental Regions. *Atmospheric Chemistry and Physics* **2012**, *12* (24), 11917–11932. https://doi.org/10.5194/acp-12-11917-2012.

(20)

Cape, J. N. Surface Ozone Concentrations and Ecosystem Health: Past Trends and a Guide to Future Projections. *Science of The Total Environment* **2008**, *400* (1–3), 257–269. https://doi.org/10.1016/j.scitotenv.2008.06.025.

(21)

Capouet, M.; Müller, J.-F. A Group Contribution Method for Estimating the Vapour Pressures of α-Pinene Oxidation Products. *Atmospheric Chemistry and Physics* **2006**, *6* (6), 1455–1467. https://doi.org/10.5194/acp-6-1455-2006.

(22)

Carlton, A. G.; Wiedinmyer, C.; Kroll, J. H. A Review of Secondary Organic Aerosol (SOA) Formation from Isoprene. *Atmos. Chem. Phys.* **2009**, *9* (14), 4987–5005. https://doi.org/10.5194/acp-9-4987-2009.

(23)

Chen, J.; Budisulistiorini, S. H.; Miyakawa, T.; Komazaki, Y.; Kuwata, M. Secondary Aerosol Formation Promotes Water Uptake by Organic-Rich Wildfire Haze Particles in Equatorial Asia. *Atmospheric Chemistry and Physics* **2018**, *18* (11), 7781–7798. https://doi.org/10.5194/acp-18-7781-2018.

(24)

Churg, A.; Brauer, M. Human Lung Parenchyma Retains PM2.5. *Am J Respir Crit Care Med* **1997**, *155* (6), 2109–2111. https://doi.org/10.1164/ajrccm.155.6.9196123.

(25)

Clegg, S. L.; Brimblecombe, P.; Wexler, A. S. Thermodynamic Model of the System H+−NH4+−SO42-−NO3-−H2O at Tropospheric Temperatures. *J. Phys. Chem. A* **1998**, *102* (12), 2137–2154. https://doi.org/10.1021/jp973042r.

(26)

Crutzen, P. J. On the Role of CH4 in Atmospheric Chemistry: Sources, Sinks and Possible Reductions in Anthropogenic Sources. *Ambio* **1995**, *24* (1), 52–55.

(27)

Dall'Osto, M.; Airs, R. L.; Beale, R.; Cree, C.; Fitzsimons, M. F.; Beddows, D.; Harrison, R. M.; Ceburnis, D.; O'Dowd, C.; Rinaldi, M.; Paglione, M.; Nenes, A.; Decesari, S.; Simó, R. Simultaneous Detection of Alkylamines in the Surface Ocean and Atmosphere of the Antarctic Sympagic Environment. *ACS Earth Space Chem.* **2019**, *3* (5), 854–862. https://doi.org/10.1021/acsearthspacechem.9b00028.

(28)

Darer, A. I.; Cole-Filipiak, N. C.; O'Connor, A. E.; Elrod, M. J. Formation And Stability Of Atmospherically Relevant Isoprene-Derived Organosulfates And Organonitrates. **2011**, 24.

(29)

Day, D. A.; Liu, S.; Russell, L. M.; Ziemann, P. J. Organonitrate Group Concentrations in Submicron Particles with High Nitrate and Organic Fractions in Coastal Southern California. *Atmospheric Environment* **2010**, *44* (16), 1970–1979. https://doi.org/10.1016/j.atmosenv.2010.02.045.

(30)

de Alcantara Lemos, J.; Oliveira, A. E. M. F. M.; Araujo, R. S.; Townsend, D. M.; Ferreira, L. A. M.; de Barros, A. L. B. Recent Progress in Micro and Nano-Encapsulation of Bioactive Derivatives of the Brazilian Genus Pterodon. *Biomedicine & Pharmacotherapy* **2021**, *143*, 112137. https://doi.org/10.1016/j.biopha.2021.112137.

(31)

De Moraes, C. M.; Lewis, W. J.; Paré, P. W.; Alborn, H. T.; Tumlinson, J. H. Herbivore-Infested Plants Selectively Attract Parasitoids. *Nature* **1998**, *393* (6685), 570–573. https://doi.org/10.1038/31219.

(32) Dockery, D. W.; Pope, C. A.; Xu, X.; Spengler, J. D.; Ware, J. H.; Fay, M. E.; Ferris, B. G.; Speizer, F. E. An Association between Air Pollution and Mortality in Six U.S. Cities. *New England Journal of Medicine* **1993**, *329* (24), 1753–1759. https://doi.org/10.1056/NEJM199312093292401.

(33) Dougherty, R. C.; Roberts, J. D.; Biros, F. J. Positive and Negative Chemical Ionization Mass Spectra of Some Aromatic Chlorinated Pesticides. *Anal. Chem.* **1975**, *47* (1), 54–59. https://doi.org/10.1021/ac60351a054.

(34) Finlayson-Pitts, B. J.; Pitts, J. N. CHAPTER 9 - Particles in the Troposphere. In *Chemistry of the Upper and Lower Atmosphere*; Finlayson-Pitts, B. J., Pitts, J. N., Eds.; Academic Press: San Diego, 2000; pp 349–435. https://doi.org/10.1016/B978-012257060-5/50011-3.

(35) Forster, P.; Storelvmo, T.; Armour, K.; Collins, W.; Dufresne, J.-L.; Frame, D.; Lunt, D. J.; Mauritsen, T.; Palmer, M. D.; Watanabe, M.; Wild, M.; Zhang, X. The Earth's Energy Budget, Climate Feedbacks, and Climate Sensitivity. In *Climate Change 2021: The Physical Science Basis. Contribution of Working Group I to the Sixth Assessment Report of the Intergovernmental Panel on Climate Change*; Masson-Delmotte, V., Zhai, P., Pirani, A., Connors, S. L., Péan, C., Berger, S., Caud, N., Chen, Y., Goldfarb, L., Gomis, M. I., Huang, M., Leitzell, K., Lonnoy, E., Matthews, J. B. R., Maycock, T. K., Waterfield, T., Yelekçi, Ö., Yu, R., Zhou, B., Eds.; Cambridge University Press: Cambridge, United Kingdom and New York, NY, USA, 2021; pp 923–1054. https://doi.org/10.1017/9781009157896.001.

(36) Fridlind, A. M.; Jacobson, M. Z. A Study of Gas-Aerosol Equilibrium and Aerosol PH in the Remote Marine Boundary Layer during the First Aerosol Characterization Experiment (ACE 1). *Journal of Geophysical Research: Atmospheres* **2000**, *105* (D13), 17325–17340. https://doi.org/10.1029/2000JD900209.

(37) Fuchs, N. A. On the Stationary Charge Distribution on Aerosol Particles in a Bipolar Ionic Atmosphere. *Geofisica Pura e Applicata* **1963**, *56* (1), 185–193. https://doi.org/10.1007/BF01993343.

(38) Gaston, C. J.; Riedel, T. P.; Zhang, Z.; Gold, A.; Surratt, J. D.; Thornton, J. A. Reactive Uptake of an Isoprene-Derived Epoxydiol to Submicron Aerosol Particles. *Environ. Sci. Technol.* **2014**, *48* (19), 11178–11186. https://doi.org/10.1021/es5034266.

(39) Gentner, D. R.; Isaacman, G.; Worton, D. R.; Chan, A. W. H.; Dallmann, T. R.; Davis, L.; Liu, S.; Day, D. A.; Russell, L. M.; Wilson, K. R.; Weber, R.; Guha, A.; Harley, R. A.; Goldstein, A. H. Elucidating Secondary Organic Aerosol from Diesel and Gasoline Vehicles through Detailed Characterization of Organic Carbon Emissions. *Proc. Natl. Acad. Sci. U.S.A.* **2012**, *109* (45), 18318–18323. https://doi.org/10.1073/pnas.1212272109.

(40) George, I. J.; Abbatt, J. P. D. Heterogeneous Oxidation of Atmospheric Aerosol Particles by Gas-Phase Radicals. *Nat Chem* **2010**, *2* (9), 713–722. https://doi.org/10.1038/nchem.806.

(41)

Goldstein, A. H.; Galbally, I. E. In the Earth's Atmosphere. 8.

(42)

Grieshop, A. P.; Donahue, N. M.; Robinson, A. L. Laboratory Investigation of Photochemical Oxidation of Organic Aerosol from Wood Fires 2: Analysis of Aerosol Mass Spectrometer Data. *Atmospheric Chemistry and Physics* **2009**, *9* (6), 2227–2240.

(43)

Grieshop, A. P.; Donahue, N. M.; Robinson, A. L. Is the Gas-Particle Partitioning in Alpha-Pinene Secondary Organic Aerosol Reversible? *Geophys. Res. Lett.* **2007**, *34* (14), L14810. https://doi.org/10.1029/2007GL029987.

(44)

Gryparis, A.; Forsberg, B.; Katsouyanni, K.; Analitis, A.; Touloumi, G.; Schwartz, J.; Samoli, E.; Medina, S.; Anderson, H. R.; Niciu, E. M.; Wichmann, H.-E.; Kriz, B.; Kosnik, M.; Skorkovsky, J.; Vonk, J. M.; Dörtbudak, Z. Acute Effects of Ozone on Mortality from the "Air Pollution and Health: A European Approach" Project. *Am J Respir Crit Care Med* **2004**, *170* (10), 1080–1087. https://doi.org/10.1164/rccm.200403-333OC.

(45)

Guenther, A. B.; Jiang, X.; Heald, C. L.; Sakulyanontvittaya, T.; Duhl, T.; Emmons, L. K.; Wang, X. The Model of Emissions of Gases and Aerosols from Nature Version 2.1 (MEGAN2.1): An Extended and Updated Framework for Modeling Biogenic Emissions. *Geoscientific Model Development* **2012**, *5* (6), 1471–1492. https://doi.org/10.5194/gmd-5-1471-2012.

(46)

Guenther, A.; Karl, T.; Harley, P.; Wiedinmyer, C.; Palmer, P. I.; Geron, C. Estimates of Global Terrestrial Isoprene Emissions Using MEGAN (Model of Emissions of Gases and Aerosols from Nature). *Atmospheric Chemistry and Physics* **2006**, *6* (11), 3181–3210. https://doi.org/10.5194/acp-6-3181-2006.

(47)

Guenther, A.; Hewitt, C. N.; Erickson, D.; Fall, R.; Geron, C.; Graedel, T.; Harley, P.; Klinger, L.; Lerdau, M.; Mckay, W. A.; Pierce, T.; Scholes, B.; Steinbrecher, R.; Tallamraju, R.; Taylor, J.; Zimmerman, P. A Global Model of Natural Volatile Organic Compound Emissions. *Journal of Geophysical Research: Atmospheres* **1995**, *100* (D5), 8873–8892. https://doi.org/10.1029/94JD02950.

(48)

Hallquist, M.; Wenger, J. C.; Baltensperger, U.; Rudich, Y.; Simpson, D.; Claeys, M.; Dommen, J.; Donahue, N. M.; George, C.; Goldstein, A. H.; Hamilton, J. F.; Herrmann, H.; Hoffmann, T.; Iinuma, Y.; Jang, M.; Jenkin, M. E.; Jimenez, J. L.; Kiendler-Scharr, A.; Maenhaut, W.; McFiggans, G.; Mentel, T. F.; Monod, A.; Prévôt, A. S. H.; Seinfeld, J. H.; Surratt, J. D.; Szmigielski, R.; Wildt, J. The Formation, Properties and Impact of Secondary Organic Aerosol: Current and Emerging Issues. *Atmospheric Chemistry and Physics* **2009**, *9* (14), 5155–5236. https://doi.org/10.5194/acp-9-5155-2009.

(49)

Harrison, R. M.; Yin, J. Particulate Matter in the Atmosphere: Which Particle Properties Are Important for Its Effects on Health? *Science of The Total Environment* **2000**, *249* (1–3), 85–101. https://doi.org/10.1016/S0048-9697(99)00513-6.

(50)

Hu, K. S.; Darer, A. I.; Elrod, M. J. Thermodynamics and Kinetics of the Hydrolysis of Atmospherically Relevant Organonitrates and Organosulfates. *Atmospheric Chemistry and Physics* **2011**, *11* (16), 8307–8320. https://doi.org/10.5194/acp-11-8307-2011.

(51)

Intra, P.; Tippayawong, N. An Overview of Differential Mobility Analyzers for Size Classification of Nanometer-Sized Aerosol Particles. **2008**, 14.

(52)

Ito, K.; De Leon, S. F.; Lippmann, M. Associations between Ozone and Daily Mortality: Analysis and Meta-Analysis. *Epidemiology* **2005**, *16* (4), 446–457.

(53)

Jacobs, M. I.; Burke, W. J.; Elrod, M. J. Kinetics of the Reactions of Isoprene-Derived Hydroxynitrates: Gas Phase Epoxide Formation and Solution Phase Hydrolysis. *Atmospheric Chemistry and Physics* **2014**, *14* (17), 8933–8946. https://doi.org/10.5194/acp-14-8933-2014.

(54)

Jefferson, A.; Eisele, F. L.; Ziemann, P. J.; Weber, R. J.; Marti, J. J.; McMurry, P. H. Measurements of the H2SO4 Mass Accommodation Coefficient onto Polydisperse Aerosol. *Journal of Geophysical Research: Atmospheres* **1997**, *102* (D15), 19021–19028. https://doi.org/10.1029/97JD01152.

(55)

Kanakidou, M.; Seinfeld, J. H.; Pandis, S. N.; Barnes, I.; Dentener, F. J.; Facchini, M. C.; Dingenen, R. V.; Ervens, B.; Nenes, A.; Nielsen, C. J.; Swietlicki, E.; Putaud, J. P.; Balkanski, Y.; Fuzzi, S.; Horth, J.; Moortgat, G. K.; Winterhalter, R.; Myhre, C. E. L.; Tsigaridis, K.; Vignati, E.; Stephanou, E. G.; Wilson, J. Organic Aerosol and Global Climate Modelling: A Review. *Atmos. Chem. Phys.* **2005**, 71.

(56)

Keene, W. C.; Pszenny, A. A. P.; Maben, J. R.; Sander, R. Variation of Marine Aerosol Acidity with Particle Size. *Geophysical Research Letters* **2002**, *29* (7), 5-1-5–4. https://doi.org/10.1029/2001GL013881.

(57)

Kercher, J. P.; Riedel, T. P.; Thornton, J. A. Chlorine Activation by N$_2$O$_5$: Simultaneous, in Situ Detection of ClNO$_2$ and N$_2$O$_5$ by Chemical Ionization Mass Spectrometry. *Atmospheric Measurement Techniques* **2009**, *2* (1), 193–204. https://doi.org/10.5194/amt-2-193-2009.

(58)

Knutson, E. O.; Whitby, K. T. Aerosol Classification by Electric Mobility: Apparatus, Theory, and Applications. *Journal of Aerosol Science* **1975**, *6* (6), 443–451. https://doi.org/10.1016/0021-8502(75)90060-9.

(59)

Krechmer, J. E.; Day, D. A.; Ziemann, P. J.; Jimenez, J. L. Direct Measurements of Gas/Particle Partitioning and Mass Accommodation Coefficients in Environmental Chambers. *Environ. Sci. Technol.* **2017**, *51* (20), 11867–11875. https://doi.org/10.1021/acs.est.7b02144.

(60)

Kroll, J. H.; Cross, E. S.; Hunter, J. F.; Pai, S.; Wallace, L. M. M.; Croteau, P. L.; Jayne, J. T.; Worsnop, D. R.; Heald, C. L.; Murphy, J. G.; Frankel, S. L. Atmospheric Evolution of Sulfur Emissions from Kīlauea: Real-Time Measurements of Oxidation, Dilution, and Neutralization within a Volcanic Plume. *Environ. Sci. Technol.* **2015**, *49* (7), 4129–4137. https://doi.org/10.1021/es506119x.

(61) Kroll, J. H.; Ng, N. L.; Murphy, S. M.; Flagan, R. C.; Seinfeld, J. H. Secondary Organic Aerosol Formation from Isoprene Photooxidation. *Environ. Sci. Technol.* **2006**, *40* (6), 1869–1877. https://doi.org/10.1021/es0524301.

(62) Lambe, A. T.; Ahern, A. T.; Williams, L. R.; Slowik, J. G.; Wong, J. P. S.; Abbatt, J. P. D.; Brune, W. H.; Ng, N. L.; Wright, J. P.; Croasdale, D. R.; Worsnop, D. R.; Davidovits, P.; Onasch, T. B. Characterization of Aerosol Photooxidation Flow Reactors: Heterogeneous Oxidation, Secondary Organic Aerosol Formation and Cloud Condensation Nuclei Activity Measurements. *Atmospheric Measurement Techniques* **2011**, *4* (3), 445–461. https://doi.org/10.5194/amt-4-445-2011.

(63) Lave, L. B.; Seskin, E. P. An Analysis of the Association between U.S. Mortality and Air Pollution. *Journal of the American Statistical Association* **1973**, *68* (342), 284–290. https://doi.org/10.1080/01621459.1973.10482421.

(64) Lee, B. H.; Lopez-Hilfiker, F. D.; Mohr, C.; Kurtén, T.; Worsnop, D. R.; Thornton, J. A. An Iodide-Adduct High-Resolution Time-of-Flight Chemical-Ionization Mass Spectrometer: Application to Atmospheric Inorganic and Organic Compounds. *Environ. Sci. Technol.* **2014**, *48* (11), 6309–6317. https://doi.org/10.1021/es500362a.

(65) Liggio, J.; Li, S.-M. Reactive Uptake of Pinonaldehyde on Acidic Aerosols. *Journal of Geophysical Research: Atmospheres* **2006**, *111* (D24). https://doi.org/10.1029/2005JD006978.

(66) Liu, X.; Day, D. A.; Krechmer, J. E.; Brown, W.; Peng, Z.; Ziemann, P. J.; Jimenez, J. L. Direct Measurements of Semi-Volatile Organic Compound Dynamics Show near-Unity Mass Accommodation Coefficients for Diverse Aerosols. *Commun Chem* **2019**, *2* (1), 1–9. https://doi.org/10.1038/s42004-019-0200-x.

(67) Liu, Y.; Monod, A.; Tritscher, T.; Praplan, A. P.; DeCarlo, P. F.; Temime-Roussel, B.; Quivet, E.; Marchand, N.; Dommen, J.; Baltensperger, U. Aqueous Phase Processing of Secondary Organic Aerosol from Isoprene Photooxidation. *Atmospheric Chemistry and Physics* **2012**, *12* (13), 5879–5895. https://doi.org/10.5194/acp-12-5879-2012.

(68) Lopez-Hilfiker, F. D.; Pospisilova, V.; Huang, W.; Kalberer, M.; Mohr, C.; Stefenelli, G.; Thornton, J. A.; Baltensperger, U.; Prevot, A. S. H.; Slowik, J. G. An Extractive Electrospray Ionization Time-of-Flight Mass Spectrometer (EESI-TOF) for Online Measurement of Atmospheric Aerosol Particles. *Atmos. Meas. Tech.* **2019**, *12* (9), 4867–4886. https://doi.org/10.5194/amt-12-4867-2019.

(69) Manning, W. J.; Godzik, B.; Musselman, R. Potential Bioindicator Plant Species for Ambient Ozone in Forested Mountain Areas of Central Europe. *Environmental Pollution* **2002**, *119* (3), 283–290. https://doi.org/10.1016/S0269-7491(02)00102-1.

(70) McKnight, E. A.; Kretekos, N. P.; Owusu, D.; LaLonde, R. L. Technical Note: Preparation and Purification of Atmospherically Relevant <I>A</I>-Hydroxynitrate Esters of

Monoterpenes. *Atmos. Chem. Phys.* **2020**, *20* (7), 4241–4254. https://doi.org/10.5194/acp-20-4241-2020.

(71)

Monks, P. S.; Granier, C.; Fuzzi, S.; Stohl, A.; Williams, M. L.; Akimoto, H.; Amann, M.; Baklanov, A.; Baltensperger, U.; Bey, I.; Blake, N.; Blake, R. S.; Carslaw, K.; Cooper, O. R.; Dentener, F.; Fowler, D.; Fragkou, E.; Frost, G. J.; Generoso, S.; Ginoux, P.; Grewe, V.; Guenther, A.; Hansson, H. C.; Henne, S.; Hjorth, J.; Hofzumahaus, A.; Huntrieser, H.; Isaksen, I. S. A.; Jenkin, M. E.; Kaiser, J.; Kanakidou, M.; Klimont, Z.; Kulmala, M.; Laj, P.; Lawrence, M. G.; Lee, J. D.; Liousse, C.; Maione, M.; McFiggans, G.; Metzger, A.; Mieville, A.; Moussiopoulos, N.; Orlando, J. J.; O'Dowd, C. D.; Palmer, P. I.; Parrish, D. D.; Petzold, A.; Platt, U.; Pöschl, U.; Prévôt, A. S. H.; Reeves, C. E.; Reimann, S.; Rudich, Y.; Sellegri, K.; Steinbrecher, R.; Simpson, D.; ten Brink, H.; Theloke, J.; van der Werf, G. R.; Vautard, R.; Vestreng, V.; Vlachokostas, Ch.; von Glasow, R. Atmospheric Composition Change – Global and Regional Air Quality. *Atmospheric Environment* **2009**, *43* (33), 5268–5350. https://doi.org/10.1016/j.atmosenv.2009.08.021.

(72)

Morales, A. C.; Jayarathne, T.; Slade, J. H.; Laskin, A.; Shepson, P. B. The Production and Hydrolysis of Organic Nitrates from OH Radical Oxidation of *β*-Ocimene. *Atmospheric Chemistry and Physics* **2021**, *21* (1), 129–145. https://doi.org/10.5194/acp-21-129-2021.

(73)

Mozurkewich, M.; McMurry, P. H.; Gupta, A.; Calvert, J. G. Mass Accommodation Coefficient for HO$_2$ Radicals on Aqueous Particles. *J. Geophys. Res.* **1987**, *92* (D4), 4163. https://doi.org/10.1029/JD092iD04p04163.

(74)

Mudway, I. S.; Kelly, F. J. Ozone and the Lung: A Sensitive Issue. *Mol Aspects Med* **2000**, *21* (1–2), 1–48. https://doi.org/10.1016/s0098-2997(00)00003-0.

(75)

Ng, N. L.; Kwan, A. J.; Surratt, J. D.; Chan, A. W. H.; Chhabra, P. S.; Sorooshian, A.; Pye, H. O. T.; Crounse, J. D.; Wennberg, P. O.; Flagan, R. C.; Seinfeld, J. H. Secondary Organic Aerosol (SOA) Formation from Reaction of Isoprene with Nitrate Radicals (NO$_3$). *Atmospheric Chemistry and Physics* **2008**, *8* (14), 4117–4140. https://doi.org/10.5194/acp-8-4117-2008.

(76)

Ng, N. L.; Brown, S. S.; Archibald, A. T.; Atlas, E.; Cohen, R. C.; Crowley, J. N.; Day, D. A.; Donahue, N. M.; Fry, J. L.; Fuchs, H.; Griffin, R. J.; Guzman, M. I.; Herrmann, H.; Hodzic, A.; Iinuma, Y.; Jimenez, J. L.; Kiendler-Scharr, A.; Lee, B. H.; Luecken, D. J.; Mao, J.; McLaren, R.; Mutzel, A.; Osthoff, H. D.; Ouyang, B.; Picquet-Varrault, B.; Platt, U.; Pye, H. O. T.; Rudich, Y.; Schwantes, R. H.; Shiraiwa, M.; Stutz, J.; Thornton, J. A.; Tilgner, A.; Williams, B. J.; Zaveri, R. A. Nitrate Radicals and Biogenic Volatile Organic Compounds: Oxidation, Mechanisms, and Organic Aerosol. *Atmos. Chem. Phys.* **2017**, *17* (3), 2103–2162. https://doi.org/10.5194/acp-17-2103-2017.

(77)

Nguyen, T. B.; Coggon, M. M.; Bates, K. H.; Zhang, X.; Schwantes, R. H.; Schilling, K. A.; Loza, C. L.; Flagan, R. C.; Wennberg, P. O.; Seinfeld, J. H. Organic Aerosol Formation from the Reactive Uptake of Isoprene Epoxydiols (IEPOX) onto Non-Acidified Inorganic Seeds. *Atmospheric Chemistry and Physics* **2014**, *14* (7), 3497–3510. https://doi.org/10.5194/acp-14-3497-2014.

(78)

Nguyen, T. B.; Roach, P. J.; Laskin, J.; Laskin, A.; Nizkorodov, S. A. Effect of Humidity on the Composition of Isoprene Photooxidation Secondary Organic Aerosol. *Atmos. Chem. Phys.* **2011**, *11* (14), 6931–6944. https://doi.org/10.5194/acp-11-6931-2011.

(79)

Pérez-Ramírez, J.; Kapteijn, F.; Schöffel, K.; Moulijn, J. A. Formation and Control of N2O in Nitric Acid Production: Where Do We Stand Today? *Applied Catalysis B: Environmental* **2003**, *44* (2), 117–151. https://doi.org/10.1016/S0926-3373(03)00026-2.

(80)

Perraud, V.; Bruns, E. A.; Ezell, M. J.; Johnson, S. N.; Yu, Y.; Alexander, M. L.; Zelenyuk, A.; Imre, D.; Chang, W. L.; Dabdub, D.; Pankow, J. F.; Finlayson-Pitts, B. J. Nonequilibrium Atmospheric Secondary Organic Aerosol Formation and Growth. *Proc Natl Acad Sci U S A* **2012**, *109* (8), 2836–2841. https://doi.org/10.1073/pnas.1119909109.

(81)

Pfrang, C.; Shiraiwa, M.; Pöschl, U. Chemical Ageing and Transformation of Diffusivity in Semi-Solid Multi-Component Organic Aerosol Particles. *Atmospheric Chemistry and Physics* **2011**, *11* (14), 7343–7354. https://doi.org/10.5194/acp-11-7343-2011.

(82)

Pinkerton, K. E.; Green, F. H.; Saiki, C.; Vallyathan, V.; Plopper, C. G.; Gopal, V.; Hung, D.; Bahne, E. B.; Lin, S. S.; Ménache, M. G.; Schenker, M. B. Distribution of Particulate Matter and Tissue Remodeling in the Human Lung. *Environ Health Perspect* **2000**, *108* (11), 1063–1069. https://doi.org/10.1289/ehp.001081063.

(83)

Pinto, R. M. A.; Salvador, J. A. R.; Le Roux, C. Bismuth(III) Salts Mediated Regioselective Ring Opening of Epoxides: An Easy Route to Halohydrins and β-Hydroxy Nitrates. *Tetrahedron* **2007**, *63* (37), 9221–9228. https://doi.org/10.1016/j.tet.2007.06.054.

(84)

Pope, C. A.; Burnett, R. T.; Thurston, G. D.; Thun, M. J.; Calle, E. E.; Krewski, D.; Godleski, J. J. Cardiovascular Mortality and Long-Term Exposure to Particulate Air Pollution: Epidemiological Evidence of General Pathophysiological Pathways of Disease. *Circulation* **2004**, *109* (1), 71–77. https://doi.org/10.1161/01.CIR.0000108927.80044.7F.

(85)

Pound, G. M. Selected Values of Evaporation and Condensation Coefficients for Simple Substances. *Journal of Physical and Chemical Reference Data* **1972**, *1* (1), 135–146. https://doi.org/10.1063/1.3253096.

(86)

Pszenny, A. a. P.; Moldanová, J.; Keene, W. C.; Sander, R.; Maben, J. R.; Martinez, M.; Crutzen, P. J.; Perner, D.; Prinn, R. G. Halogen Cycling and Aerosol PH in the Hawaiian Marine Boundary Layer. *Atmospheric Chemistry and Physics* **2004**, *4* (1), 147–168. https://doi.org/10.5194/acp-4-147-2004.

(87)

Raaschou-Nielsen, O.; Andersen, Z. J.; Beelen, R.; Samoli, E.; Stafoggia, M.; Weinmayr, G.; Hoffmann, B.; Fischer, P.; Nieuwenhuijsen, M. J.; Brunekreef, B.; Xun, W. W.; Katsouyanni, K.; Dimakopoulou, K.; Sommar, J.; Forsberg, B.; Modig, L.; Oudin, A.; Oftedal, B.; Schwarze, P. E.; Nafstad, P.; De Faire, U.; Pedersen, N. L.; Östenson, C. G.; Fratiglioni, L.; Penell, J.; Korek, M.; Pershagen, G.; Eriksen, K. T.; Sørensen, M.; Tjønneland, A.; Ellermann, T.; Eeftens,

M.; Peeters, P. H.; Meliefste, K.; Wang, M.; Bueno-de-Mesquita, B.; Key, T. J.; de Hoogh, K.; Concin, H.; Nagel, G.; Vilier, A.; Grioni, S.; Krogh, V.; Tsai, M. Y.; Ricceri, F.; Sacerdote, C.; Galassi, C.; Migliore, E.; Ranzi, A.; Cesaroni, G.; Badaloni, C.; Forastiere, F.; Tamayo, I.; Amiano, P.; Dorronsoro, M.; Trichopoulou, A.; Bamia, C.; Vineis, P.; Hoek, G. Air Pollution and Lung Cancer Incidence in 17 European Cohorts: Prospective Analyses from the European Study of Cohorts for Air Pollution Effects (ESCAPE). *The Lancet Oncology* **2013**, *14* (9), 813–822. https://doi.org/10.1016/S1470-2045(13)70279-1.

(88)

Rindelaub, J. D.; Borca, C. H.; Hostetler, M. A.; Slade, J. H.; Lipton, M. A.; Slipchenko, L. V.; Shepson, P. B. The Acid-Catalyzed Hydrolysis of an *α*-Pinene-Derived Organic Nitrate: Kinetics, Products, Reaction Mechanisms, and Atmospheric Impact. *Atmospheric Chemistry and Physics* **2016**, *16* (23), 15425–15432. https://doi.org/10.5194/acp-16-15425-2016.

(89)

Rindelaub, J. D.; McAvey, K. M.; Shepson, P. B. The Photochemical Production of Organic Nitrates from α-Pinene and Loss via Acid-Dependent Particle Phase Hydrolysis. *Atmospheric Environment* **2015**, *100*, 193–201. https://doi.org/10.1016/j.atmosenv.2014.11.010.

(90)

Rollins, A. W.; Browne, E. C.; Min, K.-E.; Pusede, S. E.; Wooldridge, P. J.; Gentner, D. R.; Goldstein, A. H.; Liu, S.; Day, D. A.; Russell, L. M.; Cohen, R. C. Evidence for NO(x) Control over Nighttime SOA Formation. *Science* **2012**, *337* (6099), 1210–1212. https://doi.org/10.1126/science.1221520.

(91)

Russell, L. M.; Bahadur, R.; Ziemann, P. J. Identifying Organic Aerosol Sources by Comparing Functional Group Composition in Chamber and Atmospheric Particles. *Proceedings of the National Academy of Sciences* **2011**, *108* (9), 3516–3521. https://doi.org/10.1073/pnas.1006461108.

(92)

Saleh, R.; Donahue, N. M.; Robinson, A. L. Time Scales for Gas-Particle Partitioning Equilibration of Secondary Organic Aerosol Formed from Alpha-Pinene Ozonolysis. *Environ. Sci. Technol.* **2013**, *47* (11), 5588–5594. https://doi.org/10.1021/es400078d.

(93)

Shiraiwa, M.; Pöschl, U. Mass Accommodation and Gas–Particle Partitioning in Secondary Organic Aerosols: Dependence on Diffusivity, Volatility, Particle-Phase Reactions, and Penetration Depth. *Atmospheric Chemistry and Physics* **2021**, *21* (3), 1565–1580. https://doi.org/10.5194/acp-21-1565-2021.

(94)

Slade, J. H.; de Perre, C.; Lee, L.; Shepson, P. B. Nitrate Radical Oxidation of *γ*-Terpinene: Hydroxy Nitrate, Total Organic Nitrate, and Secondary Organic Aerosol Yields. *Atmospheric Chemistry and Physics* **2017**, *17* (14), 8635–8650. https://doi.org/10.5194/acp-17-8635-2017.

(95)

Slusher, D. L.; Huey, L. G.; Tanner, D. J.; Flocke, F. M.; Roberts, J. M. A Thermal Dissociation–Chemical Ionization Mass Spectrometry (TD-CIMS) Technique for the Simultaneous Measurement of Peroxyacyl Nitrates and Dinitrogen Pentoxide. *Journal of Geophysical Research: Atmospheres* **2004**, *109* (D19). https://doi.org/10.1029/2004JD004670.

(96)

Sousa, T. de. *Global Implications of the Nitrogen Cycle*; Cambridge Scholars Publishing, 2020.

(97)
Surratt, J. D.; Chan, A. W. H.; Eddingsaas, N. C.; Chan, M.; Loza, C. L.; Kwan, A. J.; Hersey, S. P.; Flagan, R. C.; Wennberg, P. O.; Seinfeld, J. H. Reactive Intermediates Revealed in Secondary Organic Aerosol Formation from Isoprene. *Proceedings of the National Academy of Sciences* **2010**, *107* (15), 6640–6645. https://doi.org/10.1073/pnas.0911114107.

(98)
Surratt, J. D.; Gómez-González, Y.; Chan, A. W. H.; Vermeylen, R.; Shahgholi, M.; Kleindienst, T. E.; Edney, E. O.; Offenberg, J. H.; Lewandowski, M.; Jaoui, M.; Maenhaut, W.; Claeys, M.; Flagan, R. C.; Seinfeld, J. H. Organosulfate Formation in Biogenic Secondary Organic Aerosol. *J. Phys. Chem. A* **2008**, *112* (36), 8345–8378. https://doi.org/10.1021/jp802310p.

(99)
Sutugin, A. G.; Fuchs, N. A. Formation of Condensation Aerosols under Rapidly Changing Environmental Conditions: Theory and Method of Calculation. *Journal of Aerosol Science* **1970**, *1* (4), 287–293. https://doi.org/10.1016/0021-8502(70)90002-9.

(100)
Takeuchi, M.; Ng, N. L. Chemical Composition and Hydrolysis of Organic Nitrate Aerosol Formed from Hydroxyl and Nitrate Radical Oxidation of *α*-Pinene and *β*-Pinene. *Atmospheric Chemistry and Physics* **2019**, *19* (19), 12749–12766. https://doi.org/10.5194/acp-19-12749-2019.

(101)
Tannenbaum, H. P.; Roberts, J. David.; Dougherty, R. C. Negative Chemical Ionization Mass Spectrometry. Chloride Attachment Spectra. *Anal. Chem.* **1975**, *47* (1), 49–54. https://doi.org/10.1021/ac60351a027.

(102)
Twomey, S. Pollution and the Planetary Albedo. *Atmospheric Environment (1967)* **1974**, *8* (12), 1251–1256. https://doi.org/10.1016/0004-6981(74)90004-3.

(103)
US EPA, R. 1. *Nitrogen Oxides Control Regulations | Ground-level Ozone | New England | US EPA*. https://www3.epa.gov/region1/airquality/nox.html (accessed 2022-11-19).

(104)
Valli, H. Epidemiologic Evidence of Cardiovascular Effects of Particulate Air Pollution. *Environmental Health Perspectives* **2001**, *109*, 4.

(105)
Vander Wall, A. C.; Lakey, P. S. J.; Rossich Molina, E.; Perraud, V.; Wingen, L. M.; Xu, J.; Soulsby, D.; Gerber, R. B.; Shiraiwa, M.; Finlayson-Pitts, B. J. Understanding Interactions of Organic Nitrates with the Surface and Bulk of Organic Films: Implications for Particle Growth in the Atmosphere. *Environ. Sci.: Processes Impacts* **2018**, *20* (11), 1593–1610. https://doi.org/10.1039/C8EM00348C.

(106)
Wang, H.; Easter, R. C.; Rasch, P. J.; Wang, M.; Liu, X.; Ghan, S. J.; Qian, Y.; Yoon, J.-H.; Ma, P.-L.; Vinoj, V. Sensitivity of Remote Aerosol Distributions to Representation of Cloud–Aerosol Interactions in a Global Climate Model. *Geoscientific Model Development* **2013**, *6* (3), 765–782. https://doi.org/10.5194/gmd-6-765-2013.

(107)
Wayne, R. P.; Barnes, I.; Biggs, P.; Burrows, J. P.; Canosa-Mas, C. E.; Hjorth, J.; Le Bras, G.; Moortgat, G. K.; Perner, D.; Poulet, G.; Restelli, G.; Sidebottom, H. The Nitrate Radical:

Physics, Chemistry, and the Atmosphere. *Atmospheric Environment. Part A. General Topics* **1991**, *25* (1), 1–203. https://doi.org/10.1016/0960-1686(91)90192-A.

(108)

Wilkinson, P.; Smith, K. R.; Davies, M.; Adair, H.; Armstrong, B. G.; Barrett, M.; Bruce, N.; Haines, A.; Hamilton, I.; Oreszczyn, T.; Ridley, I.; Tonne, C.; Chalabi, Z. Public Health Benefits of Strategies to Reduce Greenhouse-Gas Emissions: Household Energy. *Lancet* **2009**, *374* (9705), 1917–1929. https://doi.org/10.1016/S0140-6736(09)61713-X.

(109)

Winkler, P. Relations Between Aerosol Acidity and Ion Balance. In *Chemistry of Multiphase Atmospheric Systems*; Jaeschke, W., Ed.; NATO ASI Series; Springer: Berlin, Heidelberg, 1986; pp 269–298. https://doi.org/10.1007/978-3-642-70627-1_11.

(110)

World Health Organization. Regional Office for South-East Asia. *Regional Health Forum, Vol. 10, No. 2*; WHO Regional Office for South-East Asia: New Delhi, 2006.

(111)

Wu, Z.; Chen, J.; Wang, Y.; Zhu, Y.; Liu, Y.; Yao, B.; Zhang, Y.; Hu, M. Interactions between Water Vapor and Atmospheric Aerosols Have Key Roles in Air Quality and Climate Change. *National Science Review* **2018**, *5* (4), 452–454. https://doi.org/10.1093/nsr/nwy063.

(112)

Xiong, F.; McAvey, K. M.; Pratt, K. A.; Groff, C. J.; Hostetler, M. A.; Lipton, M. A.; Starn, T. K.; Seeley, J. V.; Bertman, S. B.; Teng, A. P.; Crounse, J. D.; Nguyen, T. B.; Wennberg, P. O.; Misztal, P. K.; Goldstein, A. H.; Guenther, A. B.; Koss, A. R.; Olson, K. F.; de Gouw, J. A.; Baumann, K.; Edgerton, E. S.; Feiner, P. A.; Zhang, L.; Miller, D. O.; Brune, W. H.; Shepson, P. B. Observation of Isoprene Hydroxynitrates in the Southeastern United States and Implications for the Fate of NO_x. *Atmospheric Chemistry and Physics* **2015**, *15* (19), 11257–11272. https://doi.org/10.5194/acp-15-11257-2015.

(113)

Xu, C.-X.; Jere, D.; Jin, H.; Chang, S.-H.; Chung, Y.-S.; Shin, J.-Y.; Kim, J.-E.; Park, S.-J.; Lee, Y.-H.; Chae, C.-H.; Lee, K. H.; Beck, G. R.; Cho, C.-S.; Cho, M.-H. Poly(Ester Amine)-Mediated, Aerosol-Delivered Akt1 Small Interfering RNA Suppresses Lung Tumorigenesis. *Am J Respir Crit Care Med* **2008**, *178* (1), 60–73. https://doi.org/10.1164/rccm.200707-1022OC.

(114)

Xu, L.; Suresh, S.; Guo, H.; Weber, R. J.; Ng, N. L. Aerosol Characterization over the Southeastern United States Using High-Resolution Aerosol Mass Spectrometry: Spatial and Seasonal Variation of Aerosol Composition and Sources with a Focus on Organic Nitrates. *Atmospheric Chemistry and Physics* **2015**, *15* (13), 7307–7336. https://doi.org/10.5194/acp-15-7307-2015.

(115)

Zhang, B.; Shen, H.; Liu, P.; Guo, H.; Hu, Y.; Chen, Y.; Xie, S.; Xi, Z.; Skipper, T. N.; Russell, A. G. Significant Contrasts in Aerosol Acidity between China and the United States. *Atmospheric Chemistry and Physics* **2021**, *21* (10), 8341–8356. https://doi.org/10.5194/acp-21-8341-2021.

(116)

Zhang, X.; Cappa, C. D.; Jathar, S. H.; McVay, R. C.; Ensberg, J. J.; Kleeman, M. J.; Seinfeld, J. H. Influence of Vapor Wall Loss in Laboratory Chambers on Yields of Secondary Organic

Aerosol. *Proceedings of the National Academy of Sciences* **2014**, *111* (16), 5802–5807. https://doi.org/10.1073/pnas.1404727111.

(117)

Direct Measurements of Gas/Particle Partitioning and Mass Accommodation Coefficients in Environmental Chambers | Environmental Science & Technology. https://pubs.acs.org/doi/10.1021/acs.est.7b02144 (accessed 2022-12-01).

(118)

Model 3076 Constant Output Atomizer Instruction Manual. 63.

(119)

Directive 2008/101/EC of the European Parliament and of the Council of 19 November 2008 Amending Directive 2003/87/EC so as to Include Aviation Activities in the Scheme for Greenhouse Gas Emission Allowance Trading within the Community (Text with EEA Relevance); 2008; Vol. 008. http://data.europa.eu/eli/dir/2008/101/oj/eng (accessed 2022-11-19).